Nonlinear Wind Estimation using a Symmetry-Preserving Reduced-Order Observer

Jeremy W. Hopwood* and Craig A. Woolsey†
Virginia Tech, Blacksburg, VA 24061

Inferring wind velocity from aircraft motion is an enabling technology with applications in synthetic air data systems, path planning, safety monitoring, and atmospheric research. This paper presents a novel nonlinear observer for wind estimation, leveraging the symmetry of aircraft dynamics under the action of a Lie group to achieve global exponential stability guarantees. By only estimating the unmeasured wind and air-relative velocity, the reduced-order observer reduces computational complexity and simplifies nonlinear stability analysis. This approach eliminates the need for a small-perturbation assumption, reformulating the nonlinear wind estimation problem into the design of a linear, time-varying observer. Simulations with a nonlinear multirotor aircraft model demonstrate the observer's robustness to turbulence and measurement noise, highlighting its practical applicability and potential to ensure safe operation of future aircraft systems.

I. Introduction

Inferring wind velocity from aircraft motion is an enabling technology across a wide range of applications. In aeronautics, wind estimates can be used in synthetic air data systems [1, 2] and path planning algorithms [3, 4]. Furthermore, with the accuracy of wind estimates quantified [5] and/or their convergence guaranteed [6], wind estimation algorithms can be incorporated into safety monitoring systems, such as [7] and [8], to replace traditional measurement techniques. Closely tied to aviation, wind estimates are also vital to weather prediction and atmospheric science [9–12]. These areas of application have become intertwined, especially within the poorly sampled atmospheric boundary layer, with advances in the Urban/Advanced Air Mobility (UAM/AAM) mission [13, 14]. For example, the development of wind estimation technologies is important in relaxing margins for flight safety to enable more weather-tolerant operations [15, 16].

The development of model-based wind estimation algorithms has brought finer temporal resolution and greater accuracy to wind velocity estimates [6, 17–19]. These *indirect* approaches feature a low instrumentation barrier as they do not require specialized sensors, such as an anemometer, to measure wind velocity. Instead, a model of the aircraft dynamics is used in conjunction with standard navigational sensors (e.g., accelerometer, gyroscope, magnetometer, and GNSS) to continuously estimate wind velocity at the aircraft's location.

The accuracy and stability guarantees of wind estimation approaches generally fall to the severity of approximations and assumptions made. Most common is the small-perturbation assumption that allows a linear flight dynamic model to be used with a linear state estimation scheme (e.g., the Kalman filter or H_∞ filter). Even approximate nonlinear filter techniques such as the extended Kalman filter (EKF) only retain their formal guarantees for small perturbations about steady motion with sufficiently low noise [20]. For model-based wind estimation, nonlinear approaches that relax the small perturbation assumption are limited, but there have been some promising developments such as the nonlinear, passivity-based observer detailed in [6]. This approach uses the nonlinear aircraft dynamics in a passivity-based approach [21] to construct an extended state observer that is globally exponentially stable provided the aerodynamics are not highly nonlinear (e.g., stall). Another approach to overcome the limitations of linear wind estimation is the invariant extended Kalman filter [22, 23]. The invariant EKF is a type of local symmetry-preserving observer [24] which aims to expand the set of trajectories for which local stability is verified. These so-called *permanent trajectories* are a generalization of steady motions for which convergence is guaranteed.

Typical approaches to model-based wind estimation produce estimates of not only wind and air-relative velocity, but also known signals such as position, attitude, and angular velocity [25]. In many cases, there is no practical use in re-estimating this measured part of the aircraft's state using these *full-order* observers and estimators. As a result, *reduced-order* observers are of great interest in which only the unmeasured part of the state is estimated. This approach

*Ph.D. Candidate, Kevin T. Crofton Department of Aerospace and Ocean Engineering, AIAA Student Member, jeremyhopwood@vt.edu
†Professor, Kevin T. Crofton Department of Aerospace and Ocean Engineering, AIAA Associate Fellow, cwoolsey@vt.edu

can decrease computational complexity and simplify the observer design process. Furthermore, aircraft dynamics possess *symmetries*; that is, they are invariant under rotations and translations (e.g., the standard orientation of the body frame with respect to the physical airframe corresponds to just one of many valid coordinate representations). In fact, the presence of this symmetry can be exploited in the observer design to simplify convergence analysis and gain selection. Motivated by these observations, a symmetry-preserving, reduced-order observer was developed by the authors in [26], which we use here to solve the wind estimation problem.

This paper is organized as follows. Section II presents the aircraft dynamics and their invariance under rotations. Next, Section III details the design of symmetry-preserving reduced-order observers for the aircraft in wind using the theory developed in [26]. Finally, these observers are demonstrated on simulated flight data for a multirotor aircraft in Section IV, followed by concluding remarks in Section V.

II. Invariant Aircraft Dynamics in Wind

A. Rigid-Body Kinematics on $\mathsf{TSE}(3)$

Consider an aircraft, modeled as a rigid body of mass m. Let the orthonormal vectors $\{\boldsymbol{i}_1, \boldsymbol{i}_2, \boldsymbol{i}_3\}$ define an earth-fixed North-East-Down (NED) reference frame, $\mathcal{F}_{\mathrm{I}}$, which we take to be inertial over the time and space scales of vehicle motion. Let the orthonormal vectors $\{\boldsymbol{b}_1, \boldsymbol{b}_2, \boldsymbol{b}_3\}$ define the body-fixed frame, $\mathcal{F}_{\mathrm{B}}$, centered at the aircraft center of gravity (CG) with $\boldsymbol{b}_1$ out the front of the aircraft, $\boldsymbol{b}_2$ out the right-hand side, and $\boldsymbol{b}_3$ out the bottom completing the right-handed frame. The position of the body frame with respect to the inertial frame is given by the vector $\boldsymbol{q} = [x\ y\ z]^{\mathsf{T}} \in \mathbb{R}^3$. The attitude of the aircraft is described by the rotation matrix $\boldsymbol{R}_{\mathrm{IB}} \in \mathsf{SO}(3)$ that maps free vectors from $\mathcal{F}_{\mathrm{B}}$ to $\mathcal{F}_{\mathrm{I}}$. The aircraft's configuration is described by points $(\boldsymbol{q}, \boldsymbol{R}_{\mathrm{IB}})$ in the special Euclidean group, $\mathsf{SE}(3) = \mathbb{R}^3 \rtimes \mathsf{SO}(3)$, where $\rtimes$ is the semi-direct product which expresses how two elements of the group compose a new element. [27, §9.6]. Let $\boldsymbol{v} = [u\ v\ w]^{\mathsf{T}}$ and $\boldsymbol{\omega} = [p\ q\ r]^{\mathsf{T}}$ be the translational and rotational velocity of the aircraft with respect to $\mathcal{F}_{\mathrm{I}}$ expressed in $\mathcal{F}_{\mathrm{B}}$, respectively. The kinematic equations of motion are

$$\dot{\boldsymbol{q}} = \boldsymbol{R}_{\mathrm{IB}}\boldsymbol{v} \tag{1a}$$

$$\dot{\boldsymbol{R}}_{\mathrm{IB}} = \boldsymbol{R}_{\mathrm{IB}}\boldsymbol{S}(\boldsymbol{\omega}) \tag{1b}$$

where $\boldsymbol{S}(\cdot)$ is the skew-symmetric cross product equivalent matrix satisfying $\boldsymbol{S}(\boldsymbol{a})\boldsymbol{b} = \boldsymbol{a} \times \boldsymbol{b}$ for 3-vectors $\boldsymbol{a}$ and $\boldsymbol{b}$. Similarly, $\boldsymbol{S}^{-1}(\cdot)$ gives the vector whose cross product equivalent matrix is $(\cdot)$; that is, $\boldsymbol{S}^{-1}(\boldsymbol{S}(\boldsymbol{a})) = \boldsymbol{a}$. Geometrically, these kinematics are defined on the tangent bundle $\mathsf{TSE}(3) = \bigcup_{\boldsymbol{p}\in\mathsf{SE}(3)} \mathsf{T}_{\boldsymbol{p}}\mathsf{SE}(3)$, where $\mathsf{T}_{\boldsymbol{p}}\mathsf{SE}(3)$ denotes the tangent space to $\mathsf{SE}(3)$ at the point $\boldsymbol{p}$.

B. Dynamics in Steady and Uniform Wind

Since the aim is to estimate wind velocity, we now consider the aircraft dynamics in a time-varying wind field, $\boldsymbol{W} : \mathbb{R}^3 \times \mathbb{R} \to \mathbb{R}^3$, defined in the inertial frame. Let the instantaneous wind vector as experienced by the aircraft be

$$\boldsymbol{w}(t) = \boldsymbol{W}(\boldsymbol{q}(t), t) \tag{2}$$

The *apparent wind* $\boldsymbol{w}$ is taken to be part of aircraft's *extended state*. The apparent wind along with the aircraft body velocity, $\boldsymbol{v}$, define the air-relative velocity in the body frame, $\boldsymbol{v}_{\mathrm{r}}$, via the *wind triangle*

$$\boldsymbol{v}_{\mathrm{r}} = \boldsymbol{v} - \boldsymbol{R}_{\mathrm{IB}}^{\mathsf{T}}\boldsymbol{w} \tag{3}$$

For the purpose of the observer design, we assume the following.

Assumption 1. *The wind field is uniform and steady on the space and time scales considered. In other words,* $\dot{\boldsymbol{w}} = \boldsymbol{0}$.

In this case, the translational dynamics, in terms of air-relative velocity, are

$$\dot{\boldsymbol{v}}_{\mathrm{r}} = \boldsymbol{v}_{\mathrm{r}} \times \boldsymbol{\omega} + \boldsymbol{R}_{\mathrm{IB}}^{\mathsf{T}}\boldsymbol{g} + \frac{1}{m}\boldsymbol{F} \tag{4}$$

where $\boldsymbol{F}$ is the body-frame aerodynamic force and $\boldsymbol{g}$ is the gravitational acceleration vector. Letting $\boldsymbol{I}$ be the body-frame moment of inertia matrix about the center of mass and $\boldsymbol{M}$ be the aerodynamic moment in the body frame, the rotational dynamics are

$$\dot{\boldsymbol{\omega}} = \boldsymbol{I}^{-1}\left(\boldsymbol{I}\boldsymbol{\omega} \times \boldsymbol{\omega} + \boldsymbol{M}\right) \tag{5}$$

To simplify the observer design, we make the following assumption on the aircraft's aerodynamics.

Assumption 2. *The aircraft's aerodynamic force and moment satisfy*

$$\boldsymbol{F} = \boldsymbol{F}_0 + \boldsymbol{F}_v \boldsymbol{v}_{\mathrm{r}} + \boldsymbol{F}_\omega \boldsymbol{\omega} \tag{6}$$

$$\boldsymbol{M} = \boldsymbol{M}_0 + \boldsymbol{M}_v \boldsymbol{v}_{\mathrm{r}} + \boldsymbol{M}_\omega \boldsymbol{\omega} \tag{7}$$

where $\boldsymbol{F}_{(\cdot)}$ and $\boldsymbol{M}_{(\cdot)}$ are known "inputs" that vary the aircraft state and control.

This assumption might seem restrictive. However, using the force model as an example, we often consider smooth, nonlinear, quasi-steady aerodynamic models

$$\boldsymbol{F}(\boldsymbol{v}_{\mathrm{r}}, \boldsymbol{\omega}, \boldsymbol{\delta}) = \boldsymbol{F}_0(\boldsymbol{v}_{\mathrm{r}}, \boldsymbol{\omega}, \boldsymbol{\delta}) + \boldsymbol{F}_v(\boldsymbol{v}_{\mathrm{r}}, \boldsymbol{\omega}, \boldsymbol{\delta})\boldsymbol{v}_{\mathrm{r}} + \boldsymbol{F}_\omega(\boldsymbol{v}_{\mathrm{r}}, \boldsymbol{\omega}, \boldsymbol{\delta})\boldsymbol{\omega} \tag{8}$$

where $\boldsymbol{\delta}$ is the vector of flight control inputs (e.g., throttle setting and control surface deflections). Then assuming the estimates of $\boldsymbol{v}_{\mathrm{r}}$ and $\boldsymbol{\omega}$ converge much faster than $\boldsymbol{F}_{(\cdot)}$ are changing over time, Eq. (6) can be obtained by setting the arguments of $\boldsymbol{F}_{(\cdot)}$ in Eq. (8) to their best estimates at the current time. Consequences of this assumption will be explored in Section IV.

Altogether, the aircraft equations of motion used for the observer design are

$$\dot{\boldsymbol{q}} = \boldsymbol{R}_{\mathrm{IB}} \boldsymbol{v}_{\mathrm{r}} + \boldsymbol{w} \tag{9a}$$

$$\dot{\boldsymbol{R}}_{\mathrm{IB}} = \boldsymbol{R}_{\mathrm{IB}} \boldsymbol{S}(\boldsymbol{\omega}) \tag{9b}$$

$$\dot{\boldsymbol{\omega}} = \boldsymbol{I}^{-1} \left(\boldsymbol{I}\boldsymbol{\omega} \times \boldsymbol{\omega} + \boldsymbol{M}_0 + \boldsymbol{M}_v \boldsymbol{v}_{\mathrm{r}} + \boldsymbol{M}_\omega \boldsymbol{\omega} \right) \tag{9c}$$

$$\dot{\boldsymbol{v}}_{\mathrm{r}} = \boldsymbol{v}_{\mathrm{r}} \times \boldsymbol{\omega} + \boldsymbol{R}_{\mathrm{IB}}^{\mathsf{T}} \boldsymbol{g} + \frac{1}{m} \left(\boldsymbol{F}_0 + \boldsymbol{F}_v \boldsymbol{v}_{\mathrm{r}} + \boldsymbol{F}_\omega \boldsymbol{\omega} \right) \tag{9d}$$

$$\dot{\boldsymbol{w}} = \boldsymbol{0} \tag{9e}$$

Assumption 3. *The aircraft's position ($\boldsymbol{q}$), attitude ($\boldsymbol{R}_{\mathrm{IB}}$), and angular velocity ($\boldsymbol{\omega}$) are obtained with negligible error.*

Thus, we take $\boldsymbol{y} = (\boldsymbol{q}, \boldsymbol{R}_{\mathrm{IB}}, \boldsymbol{\omega}) \in \mathcal{Y} = \mathsf{SE}(3) \times \mathbb{R}^3$ to be the measured part of the state and $\boldsymbol{x} = (\boldsymbol{v}_{\mathrm{r}}, \boldsymbol{w}) \in \mathcal{X} = \mathbb{R}^n$ to be the unmeasured part. Here, the dimension of $\mathcal{Y}$ is $p = 9$ ($\mathsf{SE}(3)$ is a 6-dimensional smooth manifold), and the dimension of $\mathcal{X}$ is $n = 6$. The total state space of the system is the $(n + p = 15)$-dimensional manifold $\mathcal{X} \times \mathcal{Y}$. We will use the notation $(\boldsymbol{a}, \boldsymbol{b})$ as shorthand for $[\boldsymbol{a}^{\mathsf{T}}\ \boldsymbol{b}^{\mathsf{T}}]^{\mathsf{T}}$ if $\boldsymbol{a}$ and $\boldsymbol{b}$ are column vectors. More generally, $(\boldsymbol{a}, \boldsymbol{b})$ denotes a point in the appropriate product space in which $\boldsymbol{a}$ and $\boldsymbol{b}$ belong. With these definitions, the aircraft dynamics (9) are written as

$$\dot{\boldsymbol{x}} = \boldsymbol{f}(\boldsymbol{x}, \boldsymbol{y}, \boldsymbol{u}) \tag{10a}$$

$$\dot{\boldsymbol{y}} = \boldsymbol{h}(\boldsymbol{x}, \boldsymbol{y}, \boldsymbol{u}) \tag{10b}$$

where $\boldsymbol{u}$ is the known "input" to the system. Here, the input vector $\boldsymbol{u}$ is not necessarily flight control inputs as in the vector delta above; rather it is a collection of known quantities on which a particular transformation group acts. In this case, it is composed of all quantities, other than the system state, that are expressed in either $\mathcal{F}_{\mathrm{B}}$ or $\mathcal{F}_{\mathrm{I}}$. That is, $\boldsymbol{u} = (\boldsymbol{g}, \boldsymbol{I}, \boldsymbol{M}_0, \boldsymbol{M}_v, \boldsymbol{M}_\omega, \boldsymbol{F}_0, \boldsymbol{F}_v, \boldsymbol{F}_\omega) \in \mathcal{U}$. The vector field $(\boldsymbol{f}, \boldsymbol{h})$ in Eq. (10) is appropriately constructed from the right-hand side of Eq. (9).

C. Invariance of the Aircraft Dynamics

In order to design a symmetry-preserving observer for the aircraft in wind, we must determine what transformations of the aircraft state and input leave the dynamics (9) unchanged – that is, *invariant*. To this end, consider the following preliminaries.

1. Mathematical Preliminaries

A Lie group G is said to *act* on a manifold $\mathcal{X}$ via the mapping

$$\boldsymbol{\varphi} : G \times \mathcal{X} \to \mathcal{X},\ (g, \boldsymbol{x}) \mapsto \boldsymbol{\varphi}_g(\boldsymbol{x}) \tag{11}$$

if (i) the identity element e in G induces the identity transformation $\boldsymbol{\varphi}_e(\boldsymbol{x}) = \boldsymbol{x}$ for all $\boldsymbol{x} \in \mathcal{X}$, and (ii) the composition of group actions satisfies $\boldsymbol{\varphi}_g \circ \boldsymbol{\varphi}_h = \boldsymbol{\varphi}_{g*h}$, where "$\circ$" denotes the composition of mappings and "$*$" is group

multiplication [28, 29]. Note the inverse transformation $\boldsymbol{\varphi}_g^{-1}$ is given by the action of the inverse group element – i.e., $\boldsymbol{\varphi}_g^{-1} = \boldsymbol{\varphi}_{g^{-1}}$. With these properties, the collection $\{\boldsymbol{\varphi}_g\}_{g\in G}$ is called a *transformation group*.

As explained in [24, 28], a dynamical control system

$$\dot{\boldsymbol{x}} = \boldsymbol{f}(\boldsymbol{x}, \boldsymbol{u}) \tag{12}$$

is called *G-invariant* with respect to the transformation group $\{\boldsymbol{\varphi}_g, \boldsymbol{\psi}_g\}_{g\in G}$ if

$$\boldsymbol{f}(\boldsymbol{\varphi}_g(\boldsymbol{x}), \boldsymbol{\psi}_g(\boldsymbol{u})) = \mathrm{T}\boldsymbol{\varphi}_g(\boldsymbol{x}) \cdot \boldsymbol{f}(\boldsymbol{x}, \boldsymbol{u}) \tag{13}$$

where $\mathrm{T}\boldsymbol{\varphi}_g(\boldsymbol{x}) : \mathsf{T}_{\boldsymbol{x}}\mathcal{X} \to \mathsf{T}_{\boldsymbol{\varphi}_g(\boldsymbol{x})}\mathcal{X}$ denotes the *tangent map* of $\boldsymbol{\varphi}_g$ at $\boldsymbol{x}$ and "$\cdot$" denotes its application to a tangent vector. Note if $\mathcal{X} = \mathbb{R}^n$, then $\mathrm{T}\boldsymbol{\varphi}_g(\boldsymbol{x})$ is simply the Jacobian matrix, $\partial\boldsymbol{\varphi}_g(\boldsymbol{x})/\partial\boldsymbol{x}$.

2. $\mathsf{SO}(3)$*-Invariance of the Aircraft Dynamics in Wind*

For the reduced-order observer problem, the aim is to find a transformation group $\{\boldsymbol{\varphi}_g, \boldsymbol{\varrho}_g, \boldsymbol{\psi}_g\}_{g\in G}$ for the system (10), where $\boldsymbol{\varphi}_g$ acts on the unmeasured part of state, $\boldsymbol{\varrho}_g$ acts on the measured part, and $\boldsymbol{\psi}_g$ acts on the input. Recall Lie groups sets of elements that act on each other through group multiplication, but also topological spaces that correspond (locally) to Euclidean space. As described in Section II.A, the configuration the rigid-body aircraft is a point on such a manifold – the special Euclidean group $\mathsf{SE}(3)$. Therefore, $\mathsf{SE}(3)$ is a natural choice of Lie group G for which a transformation group is defined (like in [22, 23]). However, since position does not explicitly appear on the right-hand side of Eq. 9, choosing $G = \mathsf{SO}(3)$ to define the transformation group is sufficient for the construction of an observer.

Furthermore, we recognize the aircraft dynamics are invariant under not just a single transformation group, but rather a family of transformation groups. The two most natural choices from this family are given as follows.

Proposition 1. *The aircraft dynamics* (9) *are* $\mathsf{SO}(3)$*-invariant under the transformation groups*

$$\boldsymbol{\varphi}_g(\boldsymbol{x}) = \begin{pmatrix} \boldsymbol{v}_{\mathrm{r}} \\ \boldsymbol{R}_g\boldsymbol{w} \end{pmatrix} =: \begin{pmatrix} \boldsymbol{\varphi}_g^{v_{\mathrm{r}}}(\boldsymbol{x}) \\ \boldsymbol{\varphi}_g^{w}(\boldsymbol{x}) \end{pmatrix}$$

$$\boldsymbol{\varrho}_g(\boldsymbol{y}) = \begin{pmatrix} \boldsymbol{R}_g\boldsymbol{q} \\ \boldsymbol{R}_g\boldsymbol{R}_{\mathrm{IB}} \\ \boldsymbol{\omega} \end{pmatrix} =: \begin{pmatrix} \boldsymbol{\varrho}_g^{q}(\boldsymbol{y}) \\ \boldsymbol{\varrho}_g^{R_{\mathrm{IB}}}(\boldsymbol{y}) \\ \boldsymbol{\varrho}_g^{\omega}(\boldsymbol{y}) \end{pmatrix} \qquad \boldsymbol{\psi}_g(\boldsymbol{u}) = \begin{pmatrix} \boldsymbol{R}_g\boldsymbol{g} \\ \boldsymbol{I} \\ \boldsymbol{M}_0 \\ \boldsymbol{M}_v \\ \boldsymbol{M}_\omega \\ \boldsymbol{F}_0 \\ \boldsymbol{F}_v \\ \boldsymbol{F}_\omega \end{pmatrix} =: \begin{pmatrix} \boldsymbol{\psi}_g^{g}(\boldsymbol{u}) \\ \boldsymbol{\psi}_g^{I}(\boldsymbol{u}) \\ \boldsymbol{\psi}_g^{M_0}(\boldsymbol{u}) \\ \boldsymbol{\psi}_g^{M_v}(\boldsymbol{u}) \\ \boldsymbol{\psi}_g^{M_\omega}(\boldsymbol{u}) \\ \boldsymbol{\psi}_g^{F_0}(\boldsymbol{u}) \\ \boldsymbol{\psi}_g^{F_v}(\boldsymbol{u}) \\ \boldsymbol{\psi}_g^{F_\omega}(\boldsymbol{u}) \end{pmatrix} \tag{14.I}$$

and

$$\boldsymbol{\varphi}_g(\boldsymbol{x}) = \begin{pmatrix} \boldsymbol{R}_g\boldsymbol{v}_{\mathrm{r}} \\ \boldsymbol{w} \end{pmatrix} =: \begin{pmatrix} \boldsymbol{\varphi}_g^{v_{\mathrm{r}}}(\boldsymbol{x}) \\ \boldsymbol{\varphi}_g^{w}(\boldsymbol{x}) \end{pmatrix}$$

$$\boldsymbol{\varrho}_g(\boldsymbol{y}) = \begin{pmatrix} \boldsymbol{q} \\ \boldsymbol{R}_{\mathrm{IB}}\boldsymbol{R}_g^{\mathsf{T}} \\ \boldsymbol{R}_g\boldsymbol{\omega} \end{pmatrix} =: \begin{pmatrix} \boldsymbol{\varrho}_g^{q}(\boldsymbol{y}) \\ \boldsymbol{\varrho}_g^{R_{\mathrm{IB}}}(\boldsymbol{y}) \\ \boldsymbol{\varrho}_g^{\omega}(\boldsymbol{y}) \end{pmatrix} \qquad \boldsymbol{\psi}_g(\boldsymbol{u}) = \begin{pmatrix} \boldsymbol{g} \\ \boldsymbol{R}_g\boldsymbol{I}\boldsymbol{R}_g^{\mathsf{T}} \\ \boldsymbol{R}_g\boldsymbol{M}_0 \\ \boldsymbol{R}_g\boldsymbol{M}_v\boldsymbol{R}_g^{\mathsf{T}} \\ \boldsymbol{R}_g\boldsymbol{M}_\omega\boldsymbol{R}_g^{\mathsf{T}} \\ \boldsymbol{R}_g\boldsymbol{F}_0 \\ \boldsymbol{R}_g\boldsymbol{F}_v\boldsymbol{R}_g^{\mathsf{T}} \\ \boldsymbol{R}_g\boldsymbol{F}_\omega\boldsymbol{R}_g^{\mathsf{T}} \end{pmatrix} =: \begin{pmatrix} \boldsymbol{\psi}_g^{g}(\boldsymbol{u}) \\ \boldsymbol{\psi}_g^{I}(\boldsymbol{u}) \\ \boldsymbol{\psi}_g^{M_0}(\boldsymbol{u}) \\ \boldsymbol{\psi}_g^{M_v}(\boldsymbol{u}) \\ \boldsymbol{\psi}_g^{M_\omega}(\boldsymbol{u}) \\ \boldsymbol{\psi}_g^{F_0}(\boldsymbol{u}) \\ \boldsymbol{\psi}_g^{F_v}(\boldsymbol{u}) \\ \boldsymbol{\psi}_g^{F_\omega}(\boldsymbol{u}) \end{pmatrix} \tag{14.B}$$

where $g = \boldsymbol{R}_g \in \mathsf{SO}(3)$.

The proof of Proposition 1 is given in Appendix A.

Both transformation groups characterize the rotational symmetry of the aircraft dynamics. Since the transformation group defined by Eqs. (14.I) consists of rotations of inertial frame quantities, we call it the *inertial transformation group*. This transformation group reflects the fact that the orientation of the inertial frame is arbitrary. Conversely, Eq. (14.B) consists of rotations of body frame quantities and thus is called the *body transformation group*. Its definition recognizes that the orientation of the body frame is also arbitrary as long as parameters (e.g., aerodynamic force and moment parameters) are appropriately expressed in the rotated coordinate frame. When appropriate, we will append equation numbers with "I" or "B" when they apply to transformations groups (14.I) or (14.B), respectively.

III. Symmetry-Preserving Reduced-Order Wind Observers

Now that we have established how the dynamics (10) are $\mathsf{SO}(3)$-invariant, the theory developed by the authors in [26] can be used to obtain reduced-order observers that preserve the symmetries associated with transformation groups (14.I) and (14.B).

A. The Moving Frame

To preserve symmetries in the observer dynamics, we make use of a *moving frame* [29, Ch. 8], which can be used to find invariant functions of the system's state. The moving frame is intimately tied to how sets of transformed points $\{\boldsymbol{\varrho}_g(\boldsymbol{y}) \in \mathcal{Y} \mid g \in G\}$, called G-*orbits*, relate to the composition of Lie group actions. For our problem, we only need to consider the transformation on the measured part of the state, $\boldsymbol{\varrho}_g(\boldsymbol{y})$. Therefore, it is sufficient to consider a *moving frame* to be a mapping $\gamma : \mathcal{Y} \to G$ that has the following *equivariance* property.

$$\gamma(\boldsymbol{\varrho}_g(\boldsymbol{y})) * g = \gamma(\boldsymbol{y}) \tag{15}$$

Geometrically, the moving frame may be viewed as the map from the state space to the Lie group element that transforms points to a chosen *cross-section* – a submanifold $\mathcal{K} \subseteq \mathcal{Y}$ that transversely intersects G-orbits on $\mathcal{Y}$. This interpretation provides a method for constructing a moving frame [24, 29], which we summarize as follows. For an r-dimensional Lie group G acting freely* on the p-dimensional manifold $\mathcal{Y}$, let $\boldsymbol{\varrho}_g^{\text{inv}}$ be the part of $\boldsymbol{\varrho}_g$ that maps points $\boldsymbol{y} \in \mathcal{Y}$ to an r-dimensional submanifold of $\mathcal{Y}$ such that $\boldsymbol{\varrho}_g^{\text{inv}}$ is invertible with respect to g in a neighborhood of the identity element $e \in G$. Then, one can select a constant $\boldsymbol{k}$ in the image of $\boldsymbol{\varrho}_g^{\text{inv}}$ that defines the unique point at which the G-orbit of a generic point $\boldsymbol{y}$ intersects the $(p-r)$-dimensional cross-section $\mathcal{K}$. In other words, the moving frame is obtained by solving the *normalization equation*

$$\boldsymbol{\varrho}_h^{\text{inv}}(\boldsymbol{y}) = \boldsymbol{k} \tag{16}$$

for $h \in G$. The local solution $h = \gamma(\boldsymbol{y})$ defines the moving frame, as depicted in Figure 1.

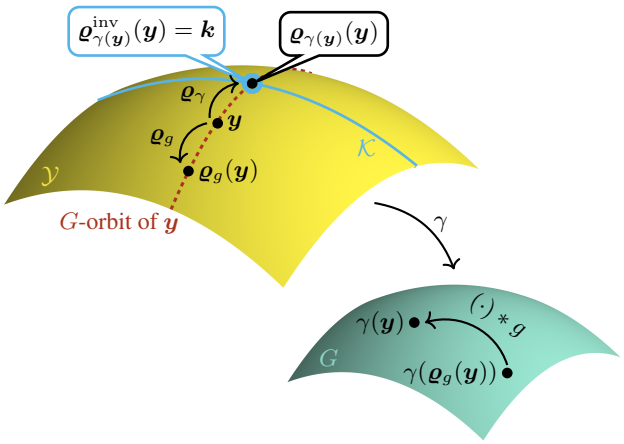

Fig. 1 Equivariance of the moving frame γ and its construction via the cross-section $\mathcal{K}$.

Since the attitude state space of the system is G itself, the *moving frame* $\gamma : \mathcal{Y} \to G$ is naturally defined by the element of $G = \mathsf{SO}(3)$ whose action on the rotational configuration yields the identity element, $e = \mathbb{I}$. Therefore, the normalization equations are

$$\boldsymbol{R}_h \boldsymbol{R}_{\text{IB}} = \mathbb{I} \tag{17.I}$$
$$\boldsymbol{R}_{\text{IB}} \boldsymbol{R}_h^{\mathsf{T}} = \mathbb{I} \tag{17.B}$$

which imply

$$h = \gamma(\boldsymbol{y}) = \boldsymbol{R}_{\text{IB}}^{\mathsf{T}} \tag{18.I}$$
$$h = \gamma(\boldsymbol{y}) = \boldsymbol{R}_{\text{IB}} \tag{18.B}$$

*The Lie group G is said to *act freely* on $\mathcal{Y}$ if $\boldsymbol{\varrho}_g(\boldsymbol{y}) = \boldsymbol{y}$ implies g is the identity element, e.

are the group elements that define moving frames with the equivariance property (15). The moving frame will be used to construct the an invariant mapping from the measured states to estimates of the unmeasured states, which is then used to define the form of the symmetry-preserving reduced-order observer (Section III.B) and obtain sufficient conditions for its stability (Section III.C).

B. Invariant Pre-Observer

With moving frames identified, we can construct symmetry-preserving reduced-order observers, defined as follows.

Definition 1 ([26]). *The dynamical system*

$$\dot{\boldsymbol{z}} = \boldsymbol{\alpha}(\boldsymbol{z}, \boldsymbol{y}, \boldsymbol{u}) \tag{19}$$

with output

$$\hat{\boldsymbol{x}} = \boldsymbol{z} + \boldsymbol{\beta}(\boldsymbol{y}) \tag{20}$$

for some smooth map $\boldsymbol{\beta} : \mathcal{Y} \to \mathcal{X}$ is a G-invariant reduced-order pre-observer if the system

$$\dot{\hat{\boldsymbol{x}}} = \boldsymbol{\alpha}(\hat{\boldsymbol{x}} - \boldsymbol{\beta}(\boldsymbol{y}), \boldsymbol{y}, \boldsymbol{u}) + \mathrm{T}\boldsymbol{\beta}(\boldsymbol{y}) \cdot \boldsymbol{h}(\boldsymbol{x}, \boldsymbol{y}, \boldsymbol{u}) \tag{21}$$

is G-invariant and the manifold

$$\mathcal{Z} = \{(\boldsymbol{z}, \boldsymbol{x}, \boldsymbol{y}) \in \mathcal{X} \times \mathcal{X} \times \mathcal{Y} \mid \boldsymbol{z} = \boldsymbol{x} - \boldsymbol{\beta}(\boldsymbol{y})\} \tag{22}$$

is positively invariant. A G-invariant pre-observer is a G-invariant observer if $\mathcal{Z}$ is asymptotically attractive.

The key to constructing the pre-observer (19) is the choice of $\boldsymbol{\beta}$, which we call the *observer map*. From Lemma 1 in [26], let

$$\boldsymbol{\beta}(\boldsymbol{y}) = \boldsymbol{\varphi}_{\gamma(\boldsymbol{y})^{-1}}\Big(\boldsymbol{\ell}\big(\boldsymbol{\varrho}_{\gamma(\boldsymbol{y})}(\boldsymbol{y})\big)\Big) \tag{23}$$

where $\boldsymbol{\ell} : \mathcal{Y} \to \mathcal{X}$ is a smooth map. As illustrated in Figure 2, this choice of $\boldsymbol{\beta}$ is special in that it commutes with the transformation group. That is,

$$\boldsymbol{\varphi}_g(\boldsymbol{\beta}(\boldsymbol{y})) = \boldsymbol{\beta}(\boldsymbol{\varrho}_g(\boldsymbol{y})) \tag{24}$$

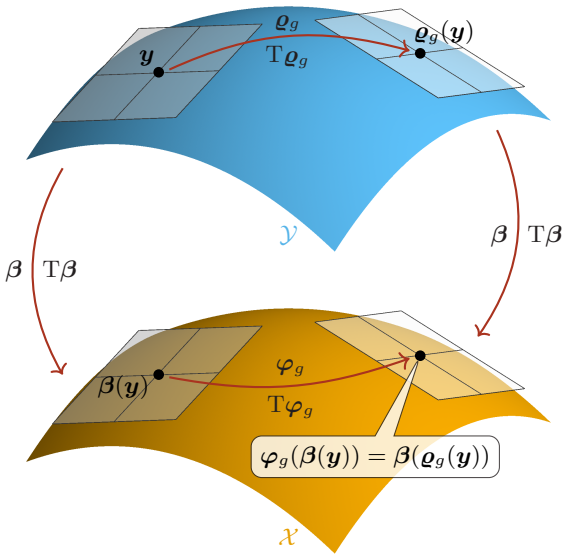

Fig. 2 Commutative relationship between $\boldsymbol{\beta}$ and the transformation group.

Inspecting the choice of $\boldsymbol{\beta}$ in Eq. (23), we notice that $\boldsymbol{\varrho}^{R_{\mathrm{IB}}}_{\gamma(\boldsymbol{y})}(\boldsymbol{y}) = \mathbb{I}$. Therefore, we need only consider $\boldsymbol{\ell} : \mathcal{Y} \setminus \mathsf{SO}(3) \to \mathcal{X}$. Let

$$\boldsymbol{\ell}(\boldsymbol{y}) = \underbrace{\begin{bmatrix} \boldsymbol{L}^q_{v_{\mathrm{r}}} & \boldsymbol{L}^\omega_{v_{\mathrm{r}}} \\ \boldsymbol{L}^q_w & \boldsymbol{L}^\omega_w \end{bmatrix}}_{\boldsymbol{L}} \begin{bmatrix} \boldsymbol{q} \\ \boldsymbol{\omega} \end{bmatrix} \tag{25}$$

where $\boldsymbol{L}$ is the *observer gain matrix* which we allow to vary with time. With this choice of $\boldsymbol{\ell}$, Eq. (23) becomes

$$\boldsymbol{\beta}(\boldsymbol{y}) = \begin{bmatrix} \boldsymbol{L}^q_{v_{\mathrm{r}}} \boldsymbol{R}^{\mathsf{T}}_{\mathrm{IB}} \boldsymbol{q} + \boldsymbol{L}^\omega_{v_{\mathrm{r}}} \boldsymbol{\omega} \\ \boldsymbol{R}_{\mathrm{IB}} \boldsymbol{L}^q_w \boldsymbol{R}^{\mathsf{T}}_{\mathrm{IB}} \boldsymbol{q} + \boldsymbol{R}_{\mathrm{IB}} \boldsymbol{L}^\omega_w \boldsymbol{\omega} \end{bmatrix} \tag{26.I}$$

$$\boldsymbol{\beta}(\boldsymbol{y}) = \begin{bmatrix} \boldsymbol{R}^{\mathsf{T}}_{\mathrm{IB}} \boldsymbol{L}^q_{v_{\mathrm{r}}} \boldsymbol{q} + \boldsymbol{R}^{\mathsf{T}}_{\mathrm{IB}} \boldsymbol{L}^\omega_{v_{\mathrm{r}}} \boldsymbol{R}_{\mathrm{IB}} \boldsymbol{\omega} \\ \boldsymbol{L}^q_w \boldsymbol{q} + \boldsymbol{L}^\omega_w \boldsymbol{R}_{\mathrm{IB}} \boldsymbol{\omega} \end{bmatrix} \tag{26.B}$$

Next, we use Theorem 1 in [26] to obtain an expression for $\boldsymbol{\alpha}$ that yields a G-invariant pre-observer.

Theorem 1 ([26])**.** *Suppose $\boldsymbol{\beta}$ is given by Eq.* (23) *and that $\boldsymbol{\varphi}_g(\boldsymbol{x})$ is linear in $\boldsymbol{x}$. Let the vector field $\boldsymbol{\alpha}(\cdot, \boldsymbol{y}, \boldsymbol{u}) : \mathcal{X} \to \mathsf{T}\mathcal{X}$ be defined by*

$$\boldsymbol{\alpha}(\boldsymbol{z}, \boldsymbol{y}, \boldsymbol{u}) = \boldsymbol{f}(\boldsymbol{z} + \boldsymbol{\beta}(\boldsymbol{y}), \boldsymbol{y}, \boldsymbol{u}) - \mathrm{T}\boldsymbol{\beta}(\boldsymbol{y}) \cdot \boldsymbol{h}(\boldsymbol{z} + \boldsymbol{\beta}(\boldsymbol{y}), \boldsymbol{y}, \boldsymbol{u}) \tag{27}$$

Then, the dynamical system (19) *with output* (20) *is a G-invariant, reduced-order pre-observer.*

Applying this theorem, we write the components of $\boldsymbol{\alpha}$ as

$$\begin{aligned} \boldsymbol{\alpha}_{v_{\mathrm{r}}}(\boldsymbol{z}, \boldsymbol{y}, \boldsymbol{u}) = \hat{\boldsymbol{v}}_{\mathrm{r}} \times \boldsymbol{\omega} + \boldsymbol{R}^{\mathsf{T}}_{\mathrm{IB}} \boldsymbol{g} + \frac{1}{m} \left(\boldsymbol{F}_0 + \boldsymbol{F}_v \hat{\boldsymbol{v}}_{\mathrm{r}} + \boldsymbol{F}_\omega \boldsymbol{\omega} \right) - \boldsymbol{L}^q_{v_{\mathrm{r}}} \boldsymbol{R}^{\mathsf{T}}_{\mathrm{IB}} \left(\boldsymbol{R}_{\mathrm{IB}} \hat{\boldsymbol{v}}_{\mathrm{r}} + \hat{\boldsymbol{w}} \right) \\ - \boldsymbol{L}^\omega_{v_{\mathrm{r}}} \boldsymbol{I}^{-1} \left(\boldsymbol{I}\boldsymbol{\omega} \times \boldsymbol{\omega} + \boldsymbol{M}_0 + \boldsymbol{M}_v \hat{\boldsymbol{v}}_{\mathrm{r}} + \boldsymbol{M}_\omega \boldsymbol{\omega} \right) + \boldsymbol{L}^q_{v_{\mathrm{r}}} \boldsymbol{S}(\boldsymbol{\omega}) \boldsymbol{R}^{\mathsf{T}}_{\mathrm{IB}} \boldsymbol{q} - \dot{\boldsymbol{L}}^q_{v_{\mathrm{r}}} \boldsymbol{R}^{\mathsf{T}}_{\mathrm{IB}} \boldsymbol{q} - \dot{\boldsymbol{L}}^\omega_{v_{\mathrm{r}}} \boldsymbol{\omega} \end{aligned} \tag{28a.I}$$

$$\begin{aligned} \boldsymbol{\alpha}_w(\boldsymbol{z}, \boldsymbol{y}, \boldsymbol{u}) = -\boldsymbol{R}_{\mathrm{IB}} \boldsymbol{L}^q_w \boldsymbol{R}^{\mathsf{T}}_{\mathrm{IB}} \left(\boldsymbol{R}_{\mathrm{IB}} \hat{\boldsymbol{v}}_{\mathrm{r}} + \hat{\boldsymbol{w}} \right) - \boldsymbol{R}_{\mathrm{IB}} \boldsymbol{L}^\omega_w \boldsymbol{I}^{-1} \left(\boldsymbol{I}\boldsymbol{\omega} \times \boldsymbol{\omega} + \boldsymbol{M}_0 + \boldsymbol{M}_v \hat{\boldsymbol{v}}_{\mathrm{r}} + \boldsymbol{M}_\omega \boldsymbol{\omega} \right) \\ - \boldsymbol{R}_{\mathrm{IB}} \boldsymbol{S}(\boldsymbol{\omega}) \boldsymbol{L}^\omega_w \boldsymbol{\omega} - \boldsymbol{R}_{\mathrm{IB}} \left(\boldsymbol{S}(\boldsymbol{\omega}) \boldsymbol{L}^q_w - \boldsymbol{L}^q_w \boldsymbol{S}(\boldsymbol{\omega}) \right) \boldsymbol{R}^{\mathsf{T}}_{\mathrm{IB}} \boldsymbol{q} - \boldsymbol{R}_{\mathrm{IB}} \dot{\boldsymbol{L}}^q_w \boldsymbol{R}^{\mathsf{T}}_{\mathrm{IB}} \boldsymbol{q} - \boldsymbol{R}_{\mathrm{IB}} \dot{\boldsymbol{L}}^\omega_w \boldsymbol{\omega} \end{aligned} \tag{28b.I}$$

and

$$\begin{aligned} \boldsymbol{\alpha}_{v_{\mathrm{r}}}(\boldsymbol{z}, \boldsymbol{y}, \boldsymbol{u}) = \hat{\boldsymbol{v}}_{\mathrm{r}} \times \boldsymbol{\omega} + \boldsymbol{R}^{\mathsf{T}}_{\mathrm{IB}} \boldsymbol{g} + \frac{1}{m} \left(\boldsymbol{F}_0 + \boldsymbol{F}_v \hat{\boldsymbol{v}}_{\mathrm{r}} + \boldsymbol{F}_\omega \boldsymbol{\omega} \right) - \boldsymbol{R}^{\mathsf{T}}_{\mathrm{IB}} \boldsymbol{L}^q_{v_{\mathrm{r}}} \left(\boldsymbol{R}_{\mathrm{IB}} \hat{\boldsymbol{v}}_{\mathrm{r}} + \hat{\boldsymbol{w}} \right) \\ - \boldsymbol{R}^{\mathsf{T}}_{\mathrm{IB}} \boldsymbol{L}^\omega_{v_{\mathrm{r}}} \boldsymbol{R}_{\mathrm{IB}} \boldsymbol{I}^{-1} \left(\boldsymbol{I}\boldsymbol{\omega} \times \boldsymbol{\omega} + \boldsymbol{M}_0 + \boldsymbol{M}_v \hat{\boldsymbol{v}}_{\mathrm{r}} + \boldsymbol{M}_\omega \boldsymbol{\omega} \right) + \boldsymbol{S}(\boldsymbol{\omega}) \boldsymbol{R}^{\mathsf{T}}_{\mathrm{IB}} \boldsymbol{L}^q_{v_{\mathrm{r}}} \boldsymbol{q} \\ + \boldsymbol{S}(\boldsymbol{\omega}) \boldsymbol{R}^{\mathsf{T}}_{\mathrm{IB}} \boldsymbol{L}^\omega_{v_{\mathrm{r}}} \boldsymbol{R}_{\mathrm{IB}} \boldsymbol{\omega} - \boldsymbol{R}^{\mathsf{T}}_{\mathrm{IB}} \dot{\boldsymbol{L}}^q_{v_{\mathrm{r}}} \boldsymbol{q} - \boldsymbol{R}^{\mathsf{T}}_{\mathrm{IB}} \dot{\boldsymbol{L}}^\omega_{v_{\mathrm{r}}} \boldsymbol{R}_{\mathrm{IB}} \boldsymbol{\omega} \end{aligned} \tag{28a.B}$$

$$\boldsymbol{\alpha}_w(\boldsymbol{z}, \boldsymbol{y}, \boldsymbol{u}) = -\boldsymbol{L}^q_w \left(\boldsymbol{R}_{\mathrm{IB}} \hat{\boldsymbol{v}}_{\mathrm{r}} + \hat{\boldsymbol{w}} \right) - \boldsymbol{L}^\omega_w \boldsymbol{R}_{\mathrm{IB}} \boldsymbol{I}^{-1} \left(\boldsymbol{I}\boldsymbol{\omega} \times \boldsymbol{\omega} + \boldsymbol{M}_0 + \boldsymbol{M}_v \hat{\boldsymbol{v}}_{\mathrm{r}} + \boldsymbol{M}_\omega \boldsymbol{\omega} \right) - \dot{\boldsymbol{L}}^q_w \boldsymbol{q} - \dot{\boldsymbol{L}}^\omega_w \boldsymbol{R}_{\mathrm{IB}} \boldsymbol{\omega} \tag{28b.B}$$

for transformation groups (14.I) and (14.B), respectively, where

$$\begin{aligned} \hat{\boldsymbol{v}}_{\mathrm{r}} &= \boldsymbol{z}_{v_{\mathrm{r}}} + \boldsymbol{L}^q_{v_{\mathrm{r}}} \boldsymbol{R}^{\mathsf{T}}_{\mathrm{IB}} \boldsymbol{q} + \boldsymbol{L}^\omega_{v_{\mathrm{r}}} \boldsymbol{\omega} \\ \hat{\boldsymbol{w}} &= \boldsymbol{z}_w + \boldsymbol{R}_{\mathrm{IB}} \boldsymbol{L}^q_w \boldsymbol{R}^{\mathsf{T}}_{\mathrm{IB}} \boldsymbol{q} + \boldsymbol{R}_{\mathrm{IB}} \boldsymbol{L}^\omega_w \boldsymbol{\omega} \end{aligned} \tag{29.I}$$

$$\begin{aligned} \hat{\boldsymbol{v}}_{\mathrm{r}} &= \boldsymbol{z}_{v_{\mathrm{r}}} + \boldsymbol{R}^{\mathsf{T}}_{\mathrm{IB}} \boldsymbol{L}^q_{v_{\mathrm{r}}} \boldsymbol{q} + \boldsymbol{R}^{\mathsf{T}}_{\mathrm{IB}} \boldsymbol{L}^\omega_{v_{\mathrm{r}}} \boldsymbol{R}_{\mathrm{IB}} \boldsymbol{\omega} \\ \hat{\boldsymbol{w}} &= \boldsymbol{z}_w + \boldsymbol{L}^q_w \boldsymbol{q} + \boldsymbol{L}^\omega_w \boldsymbol{R}_{\mathrm{IB}} \boldsymbol{\omega} \end{aligned} \tag{29.B}$$

C. Invariant Observer

We now aim to choose the gain matrix $\boldsymbol{L}$ such that the pre-observer given by Eqs. (19) and (20) is a G-invariant reduced-order *observer*. That is, we seek sufficient conditions for which the zero-error manifold $\mathcal{Z}$ is asymptotically attractive. Consider the *invariant error coordinates*

$$\boldsymbol{\eta}(\boldsymbol{z}, \boldsymbol{x}, \boldsymbol{y}) = \boldsymbol{\varphi}_{\gamma(\boldsymbol{y})}(\boldsymbol{z}) + \boldsymbol{\ell}(\boldsymbol{\varrho}_{\gamma(\boldsymbol{y})}(\boldsymbol{y})) - \boldsymbol{\varphi}_{\gamma(\boldsymbol{y})}(\boldsymbol{x}) \tag{30}$$

They are invariant in the sense that $\boldsymbol{\eta} : \mathcal{X} \times \mathcal{X} \times \mathcal{Y} \to \mathcal{X}$ is an invariant map. They are valid error coordinates because $\boldsymbol{\eta} = \mathbf{0}$ if and only if $(\boldsymbol{z}, \boldsymbol{x}, \boldsymbol{y}) \in \mathcal{Z}$, the zero-error manifold prescribed in Eq. (22).

Consider the following definitions. For any $g \in G$, let $\boldsymbol{\Lambda}_g : \mathcal{Y} \to \mathcal{X}$ be the map

$$\boldsymbol{\Lambda}_g(\boldsymbol{y}; \boldsymbol{\eta}) = \boldsymbol{\varphi}_{\boldsymbol{\varrho}_g(\boldsymbol{y})}(\boldsymbol{\eta})$$

holding $\boldsymbol{\eta}$ constant. Using the moving frame (18), let

$$\boldsymbol{X} = \boldsymbol{\varphi}_{\gamma(\boldsymbol{y})}(\boldsymbol{x}), \quad \boldsymbol{Y} = \boldsymbol{\varrho}_{\gamma(\boldsymbol{y})}(\boldsymbol{y}), \quad \boldsymbol{U} = \boldsymbol{\psi}_{\gamma(\boldsymbol{y})}(\boldsymbol{u}) \tag{31}$$

which, by construction, are invariant functions of the system state and input [29, Ch. 8]. Then, Theorem 2 of [26] gives an invariant error system whose stability is a sufficient condition for the pre-observer given by Eqs. (19) and (20) to be a G-invariant reduced-order observer; that is, $\hat{\boldsymbol{x}} \to \boldsymbol{x}$ as $t \to \infty$.

Theorem 2 ([26])**.** *Suppose the assumptions of Theorem 1 hold. The G-invariant pre-observer* (19) *is a G-invariant observer if the origin $\boldsymbol{\eta} = \mathbf{0}$ of the* invariant error system

$$\begin{aligned}\dot{\boldsymbol{\eta}} = \boldsymbol{f}(\boldsymbol{X} + \boldsymbol{\eta}, \boldsymbol{Y}, \boldsymbol{U}) - \boldsymbol{f}(\boldsymbol{X}, \boldsymbol{Y}, \boldsymbol{U}) - \mathrm{T}\boldsymbol{\beta}(\boldsymbol{Y}) \cdot \big(\boldsymbol{h}(\boldsymbol{X} + \boldsymbol{\eta}, \boldsymbol{Y}, \boldsymbol{U}) - \boldsymbol{h}(\boldsymbol{X}, \boldsymbol{Y}, \boldsymbol{U})\big) \\ + \mathrm{T}\boldsymbol{\Lambda}_{\gamma(\boldsymbol{y})}(\boldsymbol{y}; \boldsymbol{\eta}) \cdot \boldsymbol{h}(\boldsymbol{X}, \boldsymbol{Y}, \boldsymbol{U})\end{aligned} \tag{32}$$

is asymptotically stable, uniformly in $\boldsymbol{X}$, $\boldsymbol{Y}$, and $\boldsymbol{U}$.

To apply Theorem 2, we expand and simplify Eq. (32) to obtain the invariant error dynamics

$$\begin{aligned}\dot{\boldsymbol{\eta}}_{v_\mathrm{r}} &= -\boldsymbol{S}(\boldsymbol{\omega})\boldsymbol{\eta}_{v_\mathrm{r}} + \frac{1}{m}\boldsymbol{F}_v\boldsymbol{\eta}_{v_\mathrm{r}} - \boldsymbol{L}^q_{v_\mathrm{r}}(\boldsymbol{\eta}_{v_\mathrm{r}} + \boldsymbol{\eta}_w) - \boldsymbol{L}^\omega_{v_\mathrm{r}}\boldsymbol{I}^{-1}\boldsymbol{M}_v\boldsymbol{\eta}_{v_\mathrm{r}} \\ \dot{\boldsymbol{\eta}}_w &= -\boldsymbol{L}^q_w(\boldsymbol{\eta}_{v_\mathrm{r}} + \boldsymbol{\eta}_w) - \boldsymbol{L}^\omega_w\boldsymbol{I}^{-1}\boldsymbol{M}_v\boldsymbol{\eta}_{v_\mathrm{r}} - \boldsymbol{S}(\boldsymbol{\omega})\boldsymbol{\eta}_w\end{aligned} \tag{33.I}$$

$$\begin{aligned}\dot{\boldsymbol{\eta}}_{v_\mathrm{r}} &= \frac{1}{m}\boldsymbol{R}_\mathrm{IB}\boldsymbol{F}_v\boldsymbol{R}^\mathsf{T}_\mathrm{IB}\boldsymbol{\eta}_{v_\mathrm{r}} - \boldsymbol{L}^q_{v_\mathrm{r}}(\boldsymbol{\eta}_{v_\mathrm{r}} + \boldsymbol{\eta}_w) - \boldsymbol{L}^\omega_{v_\mathrm{r}}\boldsymbol{R}_\mathrm{IB}\boldsymbol{I}^{-1}\boldsymbol{M}_v\boldsymbol{R}^\mathsf{T}_\mathrm{IB}\boldsymbol{\eta}_{v_\mathrm{r}} \\ \dot{\boldsymbol{\eta}}_w &= -\boldsymbol{L}^q_w(\boldsymbol{\eta}_{v_\mathrm{r}} + \boldsymbol{\eta}_w) - \boldsymbol{L}^\omega_w\boldsymbol{R}_\mathrm{IB}\boldsymbol{I}^{-1}\boldsymbol{M}_v\boldsymbol{R}^\mathsf{T}_\mathrm{IB}\boldsymbol{\eta}_{v_\mathrm{r}}\end{aligned} \tag{33.B}$$

Notice that for the body transformation group, the transformed input signal appears as $\boldsymbol{R}_\mathrm{IB}\boldsymbol{F}_v\boldsymbol{R}^\mathsf{T}_\mathrm{IB} = \boldsymbol{U}_{F_v}$ and $\boldsymbol{R}_\mathrm{IB}\boldsymbol{I}^{-1}\boldsymbol{M}_v\boldsymbol{R}^\mathsf{T}_\mathrm{IB} = \boldsymbol{U}_I\boldsymbol{U}_{M_v}$. Also, the time derivative of the observer gain matrix does not appear in the invariant error dynamics, allowing for flexibility in its selection.

Remark 1. *The error system* (33) *depends only on the invariant error $\boldsymbol{\eta}$ and the invariants $\boldsymbol{Y}$ and $\boldsymbol{U}$ which along with $\boldsymbol{X}$ constitute a set of $n + p - r$ functionally independent invariants, $\boldsymbol{I}(\boldsymbol{x}, \boldsymbol{y}, \boldsymbol{u})$ [29, Ch. 8]. This observation is consistent with the full-order case considered in [24, Theorem 3].*

We now aim to choose the dynamics of the matrix $\boldsymbol{L}$ to render $\boldsymbol{\eta} = \mathbf{0}$ asymptotically stable. Equation (33) can be viewed as a linear, time-varying (LTV) system since $\boldsymbol{Y}$ and $\boldsymbol{U}$ are known signals. Therefore, the stabilization of the invariant error system is reduced to LTV observer design for the fictitious system

$$\begin{aligned}\dot{\boldsymbol{\xi}} &= \boldsymbol{A}(t)\boldsymbol{\xi} \\ \boldsymbol{\zeta} &= \boldsymbol{C}(t)\boldsymbol{\xi}\end{aligned} \tag{34}$$

where

$$\boldsymbol{A}(t) = \begin{bmatrix} -\boldsymbol{S}(\boldsymbol{\omega}(t)) + \boldsymbol{F}_v(t)/m & \mathbf{0} \\ \mathbf{0} & -\boldsymbol{S}(\boldsymbol{\omega}(t)) \end{bmatrix}, \qquad \boldsymbol{C}(t) = \begin{bmatrix} \mathbb{I} & \mathbb{I} \\ \boldsymbol{I}^{-1}\boldsymbol{M}_v(t) & \mathbf{0} \end{bmatrix} \tag{35.I}$$

$$\boldsymbol{A}(t) = \begin{bmatrix} \boldsymbol{R}_\mathrm{IB}(t)\boldsymbol{F}_v(t)\boldsymbol{R}^\mathsf{T}_\mathrm{IB}(t)/m & \mathbf{0} \\ \mathbf{0} & \mathbf{0} \end{bmatrix}, \qquad \boldsymbol{C}(t) = \begin{bmatrix} \mathbb{I} & \mathbb{I} \\ \boldsymbol{R}_\mathrm{IB}(t)\boldsymbol{I}^{-1}\boldsymbol{M}_v(t)\boldsymbol{R}^\mathsf{T}_\mathrm{IB}(t) & \mathbf{0} \end{bmatrix} \tag{35.B}$$

Using $\boldsymbol{L}(t)$ as the linear observer gain matrix for the system (34), the closed-loop error dynamics

$$\dot{\boldsymbol{\eta}} = (\boldsymbol{A}(t) - \boldsymbol{L}(t)\boldsymbol{C}(t))\,\boldsymbol{\eta} \tag{36}$$

are exactly the invariant error system (33). Therefore, one must simply choose positive definite matrices $\boldsymbol{Q}$ and $\boldsymbol{R}$, propagate the differential Riccati equation

$$\dot{\boldsymbol{P}}(t) = \boldsymbol{A}(t)\boldsymbol{P}(t) + \boldsymbol{P}(t)\boldsymbol{A}^{\mathsf{T}}(t) - \boldsymbol{P}(t)\boldsymbol{C}^{\mathsf{T}}(t)\boldsymbol{R}^{-1}\boldsymbol{C}(t)\boldsymbol{P}(t) + \boldsymbol{Q} \tag{37}$$

and let

$$\boldsymbol{L}(t) = \boldsymbol{P}(t)\boldsymbol{C}^{\mathsf{T}}(t)\boldsymbol{R}^{-1} \tag{38}$$

The preceding discussion proves the main result of this paper:

Theorem 3. *If the pair $(\boldsymbol{A}(t), \boldsymbol{C}(t))$ is observable, then the $\mathsf{SO}(3)$-invariant pre-observer* (19) *with $\boldsymbol{\alpha}$ given by Eq.* (27) *and $\boldsymbol{L}(t)$ satisfying Eq.* (38) *is an exponentially stable $\mathsf{SO}(3)$-invariant observer for the aircraft in wind given by Eq.* (9)*.*

The observability of $(\boldsymbol{A}(t), \boldsymbol{C}(t))$ is not overly restrictive. Most nonlinear aerodynamic models for both fixed-wing and multirotor aircraft satisfy this observability requirement. For example, constructing $\boldsymbol{F}_v$ and $\boldsymbol{M}_v$ from the large-domain fixed-wing and multirotor models given in [30] and [31], respectively, both yield observability. The theoretical results are demonstrated in simulations of a multirotor aircraft in the following section.

IV. Simulation Results

The symmetry-preserving reduced-order wind observer was implemented on simulated flight data for the small quadrotor UAV considered in [31]. Neglecting velocity-dependent inflow effects, airframe drag, and motor inertia for simplicity, we consider the following nonlinear aerodynamic model.

$$F_x = \rho\pi R^2 N_{\mathrm{r}} u_{\mathrm{r}} \left(-C_{H_{\mu_x}} R\delta t - C_{H_{\mu_0,\mu_x}} \nu_0 - C_{H_{\mu_x,\mu_z}} w_{\mathrm{r}}\right) \tag{39a}$$

$$F_y = \rho\pi R^2 N_{\mathrm{r}} v_{\mathrm{r}} \left(-C_{H_{\mu_x}} R\delta t - C_{H_{\mu_0,\mu_x}} \nu_0 - C_{H_{\mu_x,\mu_z}} w_{\mathrm{r}}\right) \tag{39b}$$

$$F_z = \rho\pi R^2 \Big(- C_{T_0} R^2 N_{\mathrm{r}} \delta^2 t + C_{T_{\mu_0}} R N_{\mathrm{r}} \nu_0 \delta t + C_{T_{\mu_z}} R\big(N_{\mathrm{r}} w_{\mathrm{r}} \delta t - p\delta a - q\delta e\big) - C_{T_{\mu_x^2}} N_{\mathrm{r}} (u_{\mathrm{r}}^2 + v_{\mathrm{r}}^2)\Big) \tag{39c}$$

$$\begin{aligned} M_x = \rho\pi R^2 \Big(& - C_{R_{\mu_x}} R^2 u_{\mathrm{r}} \delta r + C_{T_0} R^2 \delta^2 a - C_{T_{\mu_0}} R \nu_0 \delta a - C_{T_{\mu_z}} R\big(w_{\mathrm{r}} \delta a - \tfrac{1}{2}\ell^2 (N_{\mathrm{r}} p\delta t + q\delta r)\big) \\ & - C_{H_{\mu_x}} R N_{\mathrm{r}} h v_{\mathrm{r}} \delta t - C_{H_{\mu_0,\mu_x}} N_{\mathrm{r}} h v_{\mathrm{r}} \nu_0 - C_{H_{\mu_x,\mu_z}} N_{\mathrm{r}} h v_{\mathrm{r}} w_{\mathrm{r}}\Big) \end{aligned} \tag{39d}$$

$$\begin{aligned} M_y = \rho\pi R^2 \Big(& - C_{R_{\mu_x}} R^2 v_{\mathrm{r}} \delta r + C_{T_0} R^2 \delta^2 e - C_{T_{\mu_0}} R \nu_0 \delta e - C_{T_{\mu_z}} R\big(w_{\mathrm{r}} \delta e - \tfrac{1}{2}\ell^2 (N_{\mathrm{r}} q\delta t + p\delta r)\big) \\ & + C_{H_{\mu_x}} R N_{\mathrm{r}} h u_{\mathrm{r}} \delta t + C_{H_{\mu_0,\mu_x}} N_{\mathrm{r}} h u_{\mathrm{r}} \nu_0 + C_{H_{\mu_x,\mu_z}} N_{\mathrm{r}} h u_{\mathrm{r}} w_{\mathrm{r}}\Big) \end{aligned} \tag{39e}$$

$$\begin{aligned} M_z = \rho\pi R^2 \Big(& C_{Q_0} R^3 \delta^2 r + C_{Q_{\mu_0}} R^2 \nu_0 \delta r + C_{Q_{\mu_z}} R^2 \big(w_{\mathrm{r}} \delta r - p\delta e - q\delta a\big) - C_{Q_{\mu_z^2}} R N_{\mathrm{r}} \ell^2 pq \\ & - C_{H_{\mu_x}} R(u_{\mathrm{r}} \delta a + v_{\mathrm{r}} \delta e) + \tfrac{1}{2} C_{H_{\mu_x,\mu_z}} N_{\mathrm{r}} \ell^2 (u_{\mathrm{r}} p + v_{\mathrm{r}} q)\Big) \end{aligned} \tag{39f}$$

Here, ρ is the air density, R is the rotor radius, $N_{\mathrm{r}} = 4$ is the number of rotors, ν_0 is the rotor inflow velocity in hover, ℓ is the arm length, h is the height of the rotor disc above the vehicle center of gravity, and $\boldsymbol{\delta} = (\delta t, \delta a, \delta e, \delta r)$, $\boldsymbol{\delta}^2 = (\delta^2 t, \delta^2 a, \delta^2 e, \delta^2 r)$ are virtual actuators satisfying

$$\begin{bmatrix} \delta t \\ \delta a \\ \delta e \\ \delta r \end{bmatrix} = \mathbf{M_{ix}} \begin{bmatrix} \Omega_1 \\ \Omega_2 \\ \vdots \\ \Omega_{N_{\mathrm{r}}} \end{bmatrix}, \qquad \begin{bmatrix} \delta^2 t \\ \delta^2 a \\ \delta^2 e \\ \delta^2 r \end{bmatrix} = \mathbf{M_{ix}} \begin{bmatrix} \Omega_1^2 \\ \Omega_2^2 \\ \vdots \\ \Omega_{N_{\mathrm{r}}}^2 \end{bmatrix} \tag{40}$$

for motor speeds $\Omega_1, \ldots, \Omega_{N_{\mathrm{r}}}$. The mixing matrix $\mathbf{M_{ix}}$ is determined by the geometry of the aircraft (Figure 3) and is given for the quadrotor in consideration as follows:

$$\mathbf{M_{ix}} = \begin{bmatrix} \frac{1}{4} & \frac{1}{4} & \frac{1}{4} & \frac{1}{4} \\ -\ell\frac{\sqrt{2}}{2} & +\ell\frac{\sqrt{2}}{2} & +\ell\frac{\sqrt{2}}{2} & -\ell\frac{\sqrt{2}}{2} \\ +\ell\frac{\sqrt{2}}{2} & -\ell\frac{\sqrt{2}}{2} & +\ell\frac{\sqrt{2}}{2} & -\ell\frac{\sqrt{2}}{2} \\ +1 & +1 & -1 & -1 \end{bmatrix} \tag{41}$$

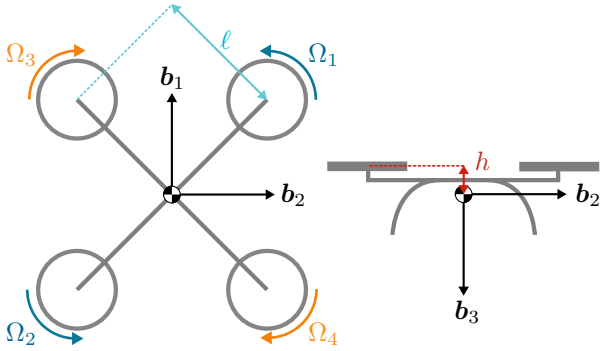

Fig. 3 Quadrotor geometry.

Note that $\boldsymbol{\delta}$ and $\boldsymbol{\delta}^2$ are not controlled independently; rather they are related through $\mathbf{M_{ix}}$. Therefore, we consider $\boldsymbol{\delta}$ to be the control input.

The tuning parameters $\boldsymbol{Q}$ and $\boldsymbol{R}$ can be selected in a number of ways, albeit less intuitively than a linear quadratic regulator or a Kalman-Bucy filter since the state and output of the LTV system (34) do not hold similar physical meaning. In this work, we chose to select $\boldsymbol{Q}$ and $\boldsymbol{R}$ using an inverse optimality approach. Let $\boldsymbol{A}_0$ and $\boldsymbol{C}_0$ be the constant matrices defined by evaluating Eq. (35) at hover (or any other nominal flight condition). Then, choose a gain matrix $\boldsymbol{L}_{\text{pp}}$ to place the poles of the LTI nominal error system $\dot{\boldsymbol{\eta}} = (\boldsymbol{A}_0 - \boldsymbol{L}_{\text{pp}}\boldsymbol{C}_0)\boldsymbol{\eta}$ at some desired location. We chose to place the poles in a first-order low-pass Butterworth configuration with a cutoff frequency of 4 rad/s. Let $\boldsymbol{L}_0 = \boldsymbol{P}_0\boldsymbol{C}_0^{\mathsf{T}}\boldsymbol{R}^{-1}$ where $\boldsymbol{P}_0$ satisfies the algebraic Riccati equation $\boldsymbol{A}_0\boldsymbol{P}_0 + \boldsymbol{P}_0\boldsymbol{A}_0^{\mathsf{T}} - \boldsymbol{P}_0\boldsymbol{C}_0^{\mathsf{T}}\boldsymbol{R}^{-1}\boldsymbol{C}_0\boldsymbol{P}_0 + \boldsymbol{Q} = \boldsymbol{0}$. Using a constrained optimization solver, the inverse optimality problem is solved by numerically finding $\boldsymbol{Q}$ and $\boldsymbol{R}$ that minimize the cost function

$$J = \frac{1}{2}\,\text{Tr}\left[(\boldsymbol{L}_0 - \boldsymbol{L}_{\text{pp}})^{\mathsf{T}}(\boldsymbol{L}_0 - \boldsymbol{L}_{\text{pp}})\right] \tag{42}$$

while constraining $\boldsymbol{Q}$ and $\boldsymbol{R}$ to be positive definite and norm bounded (e.g., $\|\boldsymbol{Q}\| \leq 100$ and $\|\boldsymbol{R}\| \leq 100$). This tuning approach was found to yield favorable results across many simulation scenarios. All results below were obtained using

$$\boldsymbol{Q} = \begin{bmatrix} 90.8 & 0 & 0 & 0 & 0 & 0 \\ 0 & 90.8 & 0 & 0 & 0 & 0 \\ 0 & 0 & 36.4 & 0 & 0 & -23.8 \\ 0 & 0 & 0 & 90.8 & 0 & 0 \\ 0 & 0 & 0 & 0 & 90.8 & 0 \\ 0 & 0 & -23.8 & 0 & 0 & 80.4 \end{bmatrix}, \quad \boldsymbol{R} = \begin{bmatrix} 11.4 & 0 & 0 & 0 & -2.0 & 0 \\ 0 & 11.4 & 0 & -2.1 & 0 & 0 \\ 0 & 0 & 7.0 & 0 & 0 & 0 \\ 0 & -2.1 & 0 & 0.8 & 0 & 0 \\ -2.0 & 0 & 0 & 0 & 0.7 & 0 \\ 0 & 0 & 0 & 0 & 0 & 50.3 \end{bmatrix} \tag{43}$$

A. Demonstration of Theoretical Guarantees

The symmetry-preserving reduced-order wind observers detailed in Section III were first implemented in simulation with all assumptions satisfied in order to demonstrate the theoretical convergence guarantees. That is, the aerodynamic force and moment perfectly satisfy Assumption 2 and the wind is constant, satisfying Assumption 1. For this ideal case, we decompose the nonlinear aerodynamic model in Eq. 39 according to Eq. (8) and evaluate the argument $\boldsymbol{v}_{\text{r}}$ in $\boldsymbol{F}_0$, $\boldsymbol{F}_v$, etc. to a nominal value of zero. Note this only affects the few terms in Eq. (39) that are nonlinear in air-relative velocity. The aircraft dynamics with the idealized aerodynamic model were simulated in a uniform wind field with components $W_{\text{N}} = 10$ m/s, $W_{\text{E}} = -10$ m/s, and $W_{\text{D}} = 0$ m/s using MATLAB. To showcase the nonlinear stability guarantees and global nature of the observer, a large-amplitude multisine input excitation was injected on top of the feedback control signal (Figure 4a). The multisine was constructed with frequencies ranging from 0.01 to 1 Hz to effectively explore the state space as seen in Figure 4.

The observability condition of Theorem 3 was verified for the simulated trajectory. The LTV observability Gramian $\boldsymbol{G}_o(t_0, t_f)$ was numerically constructed backwards in time from $t_f = 20$ to $t_0 = 0$. As shown in Figure 5, the minimum eigenvalue of the observability Gramian is bounded away from zero backwards in time, implying observability of $(\boldsymbol{A}(t), \boldsymbol{C}(t))$ on the interval $[t_0, 20)$ for any $t_0 \geq 0$ [32, Ch. 9]. Due to the structure of $\boldsymbol{A}$ and $\boldsymbol{C}$, the minimum eigenvalue $\lambda_{\min}(\boldsymbol{G}_o)$ is the same for both transformation groups. Also shown in Figure 5 is the minimum eigenvalue of

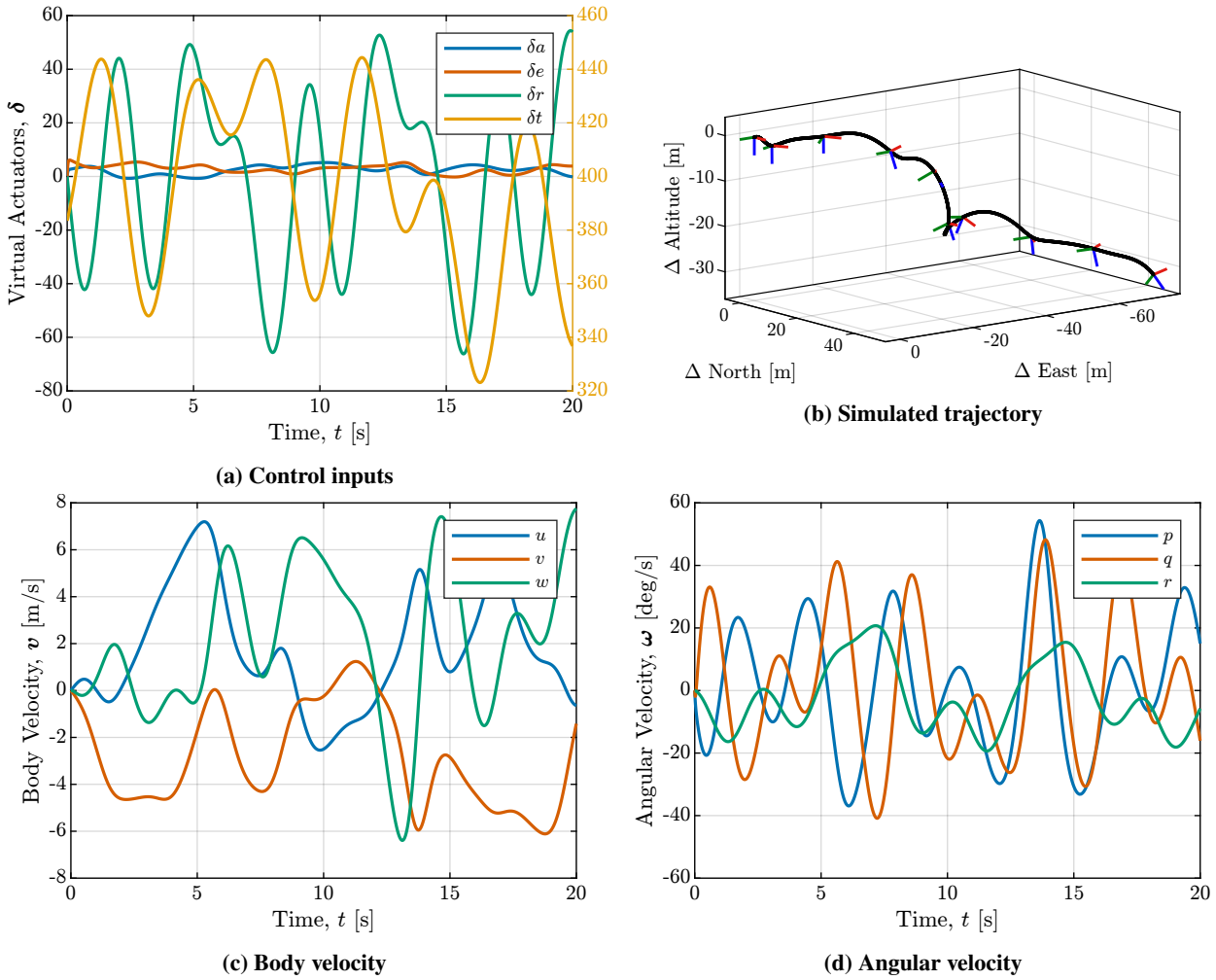

(a) Control inputs

(b) Simulated trajectory

(c) Body velocity

(d) Angular velocity

Fig. 4 Ideal simulation in uniform wind.

the observability Gramian for the nominal hover flight condition in zero wind, showing persistent maneuvering is not a requirement for this observer.

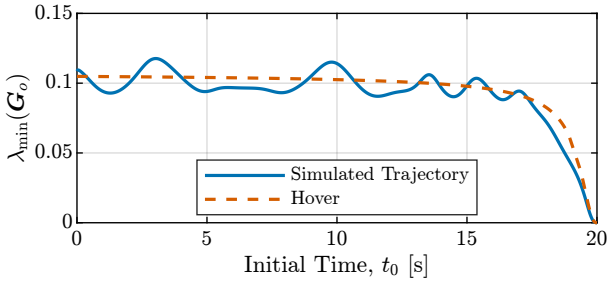

Fig. 5 Minimum eigenvalue of the LTV observability Gramian on the interval $[t_0, 20]$.

Next, the observers for both the inertial and body transformation groups were numerically simulated. The resulting estimates of air-relative and wind velocity are shown in Figures 6 and 7, respectively. These results demonstrate the guaranteed exponential convergence despite large variations in the aircraft state. Since all assumptions were satisfied, the observers designed using both transformation groups yielded nearly identical results. This parity is expected since the same rotational symmetry of the dynamics is equivalently preserved – just from the viewpoint of different reference

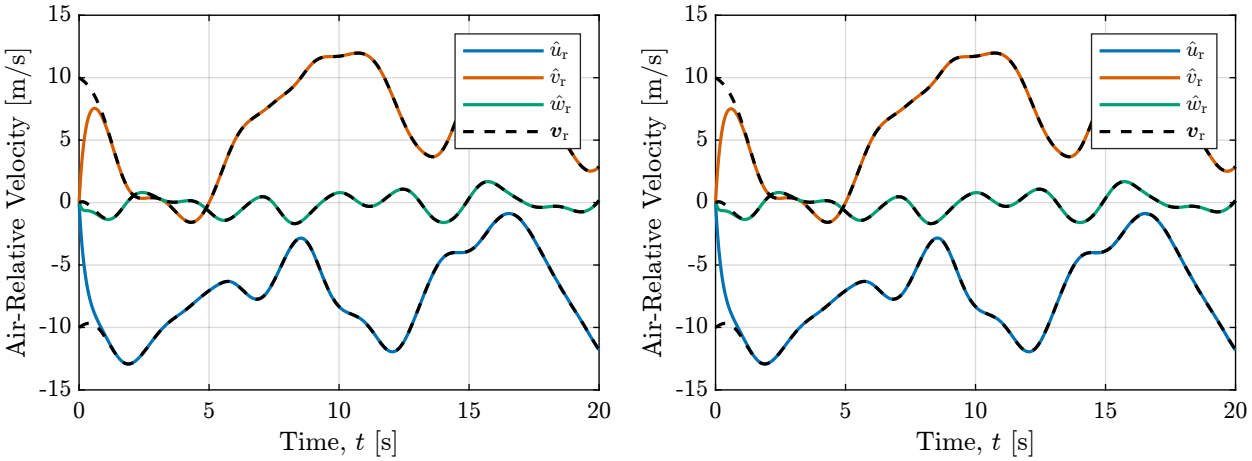

(a) Inertial transformation group **(b) Body transformation group**

Fig. 6 Estimated air-relative velocity (ideal case).

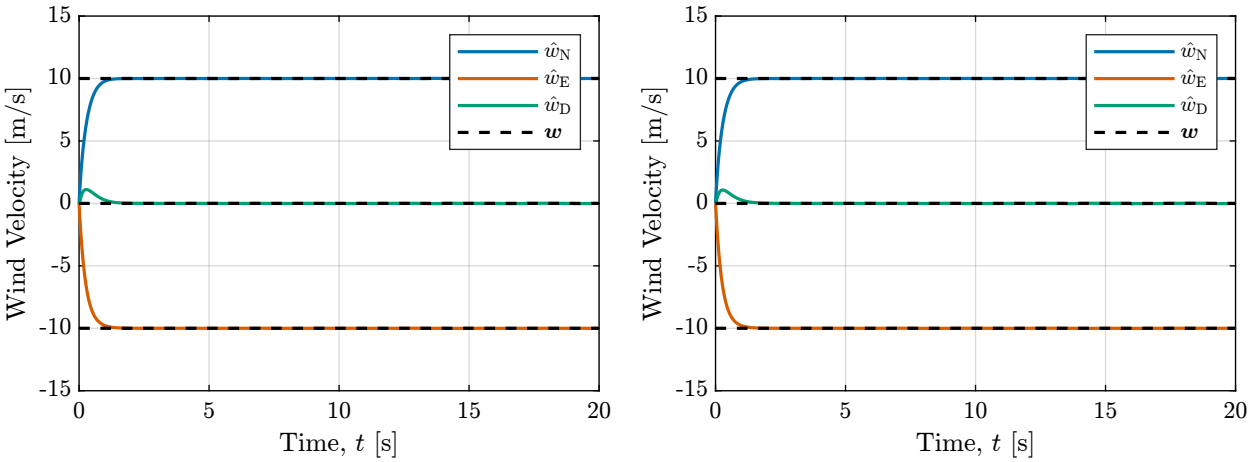

(a) Inertial transformation group **(b) Body transformation group**

Fig. 7 Estimated wind velocity (ideal case).

frames. The practical difference between using transformation groups (14.I) and (14.B) is the coordinate frame in which the observer mapping $\boldsymbol{\ell}$ is expressed.

B. Robustness Analysis

To explore the differences between transformation groups (14.I) and (14.B) and to stress the proposed observer, the aircraft was simulated in Von Kármán turbulence using the full nonlinear aerodynamic model (39), violating Assumptions 1 and 2. Additionally, Assumption 3 was violated by introducing measurement noise (the same realization for all simulations). Specifically, the measurements of $\boldsymbol{q}$, $\boldsymbol{R}_{\mathrm{IB}}$, and $\boldsymbol{\omega}$ respectively satisfied

$$\boldsymbol{y}_q = \boldsymbol{q} + \tilde{\boldsymbol{w}}_q, \quad \boldsymbol{y}_{R_{\mathrm{IB}}} = \boldsymbol{R}_{\mathrm{IB}} \exp(\boldsymbol{S}(\tilde{\boldsymbol{w}}_{R_{\mathrm{IB}}})), \quad \boldsymbol{y}_\omega = \boldsymbol{\omega} + \tilde{\boldsymbol{w}}_\omega \tag{44}$$

where $\tilde{\boldsymbol{w}}_q$, $\tilde{\boldsymbol{w}}_{R_{\mathrm{IB}}}$, and $\tilde{\boldsymbol{w}}_\omega$, are zero-mean, Gaussian, continuous-time, white noise with power spectral densities $2 \times 10^{-3}\mathbb{I}\ \frac{\mathrm{m}^2}{\mathrm{Hz}}$, $10^{-6}\mathbb{I}\ \frac{1}{\mathrm{Hz}}$, and $5 \times 10^{-6}\mathbb{I}\ \frac{(\mathrm{rad/s})^2}{\mathrm{Hz}}$, respectively. Since the transient performance and steady state accuracy of all components of air-relative and wind velocity estimates were similar, we only discuss the North component of wind velocity. The results for this scenario are shown in Figure 8a, were we see that measurement noise corrupts the resulting estimate but does not cause an unbounded response. For comparison, the same simulation scenario with

measurement noise removed is shown in Figure 8b. Here, we see good tracking of the fluctuations in wind velocity – an important aim in this work. While proof of stability for this case is beyond the scope of this paper, the results shown are indicative of the observer's inherent robustness to disturbances, as expected from the fact that the undisturbed invariant error system is globally exponentially stable [33, Lemma 5.1]. The observer's robustness to turbulence and modeling error is considered from the stochastic perspective in [34].

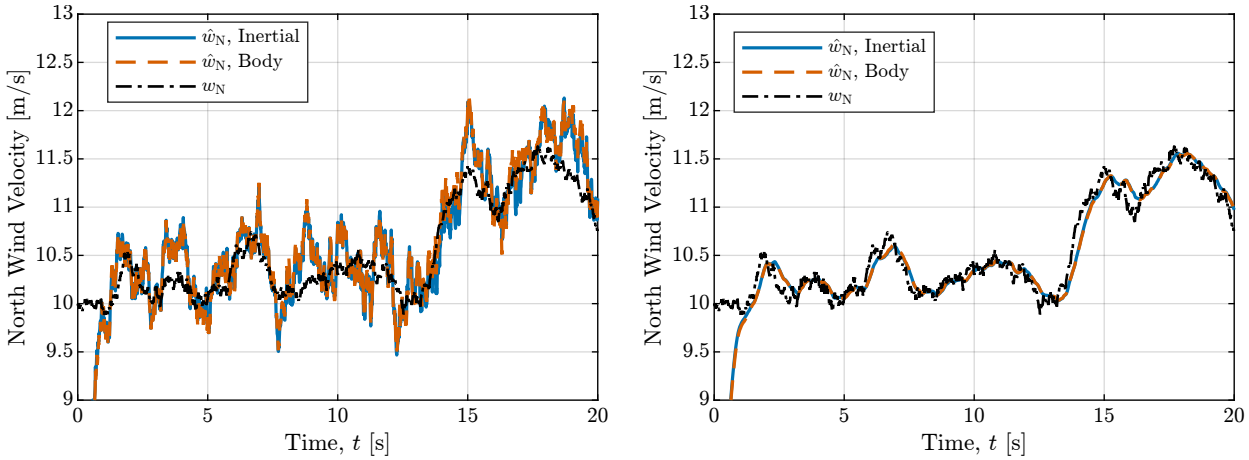

(a) With measurement noise **(b) No measurement noise**

Fig. 8 Estimated North wind velocity using full nonlinear aerodynamic model with Kármán turbulence.

One caveat about the proposed observer is that care must be taken in its numerical implementation. For example, it was found the use of a fixed-step Runge-Kutta integration scheme necessitated very small time steps (10^{-4} seconds). This issue may be alleviated by using adaptive step sizing as well as methods that leverage the Jacobian of the observer dynamics. A similar problem encountered in practical implementation is that position data is often available at a much lower rate than gyro and attitude data. To investigate, a comparison among position data rates of 8 Hz, 20 Hz, and 50 Hz was conducted using the idealized simulation discussed in Section IV.A. The results for the North wind velocity estimate are shown in Figure 9. In this case, the most recent position data was held constant between samples. As the sampling rate increases, we recover the continuous-time results. To improve performance for sampled data, predictions of position should be propagated between samples. This is an inexpensive computation and is expected to greatly improve accuracy.

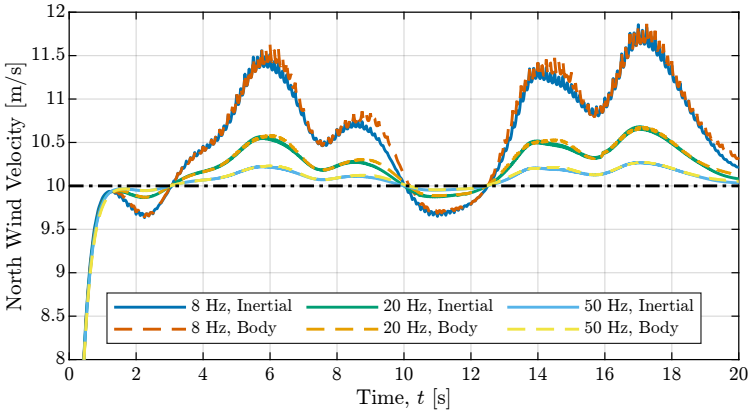

Fig. 9 North wind velocity estimate using sampled position data.

From these results, the benefit of using one transformation group over another is not apparent. To quantify the small difference between transformation groups, the L_2 norm of the estimate error, $\|\hat{\boldsymbol{x}} - \boldsymbol{x}\|_{L_2} = (\int_{t_0}^{t_f} \|\hat{\boldsymbol{x}}(t) - \boldsymbol{x}(t)\|^2)^{1/2}$, was computed and is tabulated in Table 1. Across all the simulation scenarios considered, the inertial transformation group produced marginally more accurate estimates.

Table 1 L_2 **Norm of Estimate Error,** $\|\hat{\boldsymbol{x}} - \boldsymbol{x}\|_{L_2}$

	Transformation Group	
Simulation Scenario	Inertial	Body
Ideal (Figure 7)	2.36	2.38
Von Kármán plus Noise (Figure 8a)	3.99	4.04
Von Kármán (Figure 8b)	3.45	3.47
8 Hz Position Data (Figure 9)	5.65	5.71
20 Hz Position Data (Figure 9)	3.94	3.98
50 Hz Position Data (Figure 9)	3.06	3.09

V. Conclusions

A novel symmetry-preserving, reduced-order observer has been applied to the problem of wind estimation from aircraft motion. The proposed observer does not rely on a small-perturbation assumption, bur rather exploits the invariance of the aircraft dynamics under rotations to ensure exponential convergence of the estimate. Furthermore, the reduced-order formulation does not re-estimate known parts of the state vector, reducing computational complexity and simplifying tuning. Two different transformation groups were considered and were found to both produce accurate estimates even when the assumptions of the observer were violated. Quantitative analysis of the state estimate error showed the observer designed using the inertial transformation group gave slightly more accurate results. Critically, this provably stable observer provides strong guarantees that can be incorporated into a wide variety of applications, such as synthetic air data systems, path planning algorithms, safety monitoring solutions, and numerical weather models.

A. Proof of Proposition 1

Note that the tangent maps of the transformation groups (14.I) and (14.B) at $(\boldsymbol{x}, \boldsymbol{y}, \boldsymbol{u})$ applied to $\boldsymbol{f}(\boldsymbol{x}, \boldsymbol{y}, \boldsymbol{u})$ and $\boldsymbol{h}(\boldsymbol{x}, \boldsymbol{y}, \boldsymbol{u})$ respectively satisfy

$$\mathrm{T}\boldsymbol{\varphi}_g(\boldsymbol{x}) \cdot \boldsymbol{f}(\boldsymbol{x}, \boldsymbol{y}, \boldsymbol{u}) = \begin{pmatrix} \boldsymbol{f}_{v_\mathrm{r}}(\boldsymbol{x}, \boldsymbol{u}) \\ \boldsymbol{R}_g \boldsymbol{f}_w(\boldsymbol{x}, \boldsymbol{u}) \end{pmatrix} \quad \text{and} \quad \mathrm{T}\boldsymbol{\varrho}_g(\boldsymbol{y}) \cdot \boldsymbol{h}(\boldsymbol{x}, \boldsymbol{y}, \boldsymbol{u}) = \begin{pmatrix} \boldsymbol{R}_g \boldsymbol{f}_q(\boldsymbol{x}, \boldsymbol{u}) \\ \boldsymbol{R}_g \boldsymbol{f}_{R_\mathrm{IB}}(\boldsymbol{x}, \boldsymbol{u}) \\ \boldsymbol{f}_\omega(\boldsymbol{x}, \boldsymbol{u}) \end{pmatrix} \tag{45.I}$$

$$\mathrm{T}\boldsymbol{\varphi}_g(\boldsymbol{x}) \cdot \boldsymbol{f}(\boldsymbol{x}, \boldsymbol{y}, \boldsymbol{u}) = \begin{pmatrix} \boldsymbol{R}_g \boldsymbol{f}_{v_\mathrm{r}}(\boldsymbol{x}, \boldsymbol{u}) \\ \boldsymbol{f}_w(\boldsymbol{x}, \boldsymbol{u}) \end{pmatrix} \quad \text{and} \quad \mathrm{T}\boldsymbol{\varrho}_g(\boldsymbol{y}) \cdot \boldsymbol{h}(\boldsymbol{x}, \boldsymbol{y}, \boldsymbol{u}) = \begin{pmatrix} \boldsymbol{f}_q(\boldsymbol{x}, \boldsymbol{u}) \\ \boldsymbol{f}_{R_\mathrm{IB}}(\boldsymbol{x}, \boldsymbol{u}) \boldsymbol{R}_g^\mathsf{T} \\ \boldsymbol{R}_g \boldsymbol{f}_\omega(\boldsymbol{x}, \boldsymbol{u}) \end{pmatrix} \tag{45.B}$$

We must show that the expressions above are equal to the evaluation of $\boldsymbol{f}$ and $\boldsymbol{h}$ at the transformed point $(\boldsymbol{\varphi}_g(\boldsymbol{x}), \boldsymbol{\varrho}_g(\boldsymbol{u}), \boldsymbol{\psi}_g(\boldsymbol{u}))$. Starting with the relative velocity dynamics, we have

$$\boldsymbol{f}_{v_\mathrm{r}}(\boldsymbol{\varphi}_g(\boldsymbol{x}), \boldsymbol{\varrho}_g(\boldsymbol{y}), \boldsymbol{\psi}_g(\boldsymbol{u})) = \boldsymbol{v}_\mathrm{r} \times \boldsymbol{\omega} + \boldsymbol{R}_\mathrm{IB}^\mathsf{T} \boldsymbol{R}_g^\mathsf{T} \boldsymbol{R}_g \boldsymbol{g} + \frac{1}{m} (\boldsymbol{F}_0 + \boldsymbol{F}_v \boldsymbol{v}_\mathrm{r} + \boldsymbol{F}_\omega \boldsymbol{\omega}) = \boldsymbol{f}_{v_\mathrm{r}}(\boldsymbol{x}, \boldsymbol{y}, \boldsymbol{u}) \tag{46.I}$$

$$\begin{aligned} \boldsymbol{f}_{v_\mathrm{r}}(\boldsymbol{\varphi}_g(\boldsymbol{x}), \boldsymbol{\varrho}_g(\boldsymbol{y}), \boldsymbol{\psi}_g(\boldsymbol{u})) &= \boldsymbol{R}_g \boldsymbol{v}_\mathrm{r} \times \boldsymbol{R}_g \boldsymbol{\omega} + \boldsymbol{R}_g \boldsymbol{R}_\mathrm{IB}^\mathsf{T} \boldsymbol{g} + \frac{1}{m} \left(\boldsymbol{R}_g \boldsymbol{F}_0 + \boldsymbol{R}_g \boldsymbol{F}_v \boldsymbol{R}_g^\mathsf{T} \boldsymbol{R}_g \boldsymbol{v}_\mathrm{r} + \boldsymbol{R}_g \boldsymbol{F}_\omega \boldsymbol{R}_g^\mathsf{T} \boldsymbol{R}_g \boldsymbol{\omega} \right) \\ &= \boldsymbol{R}_g \left(\boldsymbol{v}_\mathrm{r} \times \boldsymbol{\omega} + \boldsymbol{R}_\mathrm{IB}^\mathsf{T} \boldsymbol{g} + \frac{1}{m} (\boldsymbol{F}_0 + \boldsymbol{F}_v \boldsymbol{v}_\mathrm{r} + \boldsymbol{F}_\omega \boldsymbol{\omega}) \right) \\ &= \boldsymbol{R}_g \boldsymbol{f}_{v_\mathrm{r}}(\boldsymbol{x}, \boldsymbol{y}, \boldsymbol{u}) \end{aligned} \tag{46.B}$$

The invariance of the apparent wind velocity dynamics $\dot{\boldsymbol{w}} = \boldsymbol{0}$ is trivially satisfied. For the position kinematics, we write

$$\boldsymbol{f}_q(\boldsymbol{\varphi}_g(\boldsymbol{x}), \boldsymbol{\varrho}_g(\boldsymbol{y}), \boldsymbol{\psi}_g(\boldsymbol{u})) = \boldsymbol{R}_g \boldsymbol{R}_\mathrm{IB} \boldsymbol{v}_\mathrm{r} + \boldsymbol{R}_g \boldsymbol{w} = \boldsymbol{R}_g \boldsymbol{f}_q(\boldsymbol{x}, \boldsymbol{y}, \boldsymbol{u}) \tag{47.I}$$

$$\boldsymbol{f}_q(\boldsymbol{\varphi}_g(\boldsymbol{x}), \boldsymbol{\varrho}_g(\boldsymbol{y}), \boldsymbol{\psi}_g(\boldsymbol{u})) = \boldsymbol{R}_\mathrm{IB} \boldsymbol{R}_g^\mathsf{T} \boldsymbol{R}_g \boldsymbol{v}_\mathrm{r} + \boldsymbol{w} = \boldsymbol{f}_q(\boldsymbol{x}, \boldsymbol{y}, \boldsymbol{u}) \tag{47.B}$$

The attitude kinematics at the transformed point satisfy

$$\boldsymbol{f}_{R_{\mathrm{IB}}}(\boldsymbol{\varphi}_g(\boldsymbol{x}), \boldsymbol{\varrho}_g(\boldsymbol{y}), \boldsymbol{\psi}_g(\boldsymbol{u})) = \boldsymbol{R}_g \boldsymbol{R}_{\mathrm{IB}} \boldsymbol{S}(\boldsymbol{\omega}) = \boldsymbol{R}_g \boldsymbol{f}_{R_{\mathrm{IB}}}(\boldsymbol{x}, \boldsymbol{y}, \boldsymbol{u}) \tag{48.I}$$

$$\begin{aligned} \boldsymbol{f}_{R_{\mathrm{IB}}}(\boldsymbol{\varphi}_g(\boldsymbol{x}), \boldsymbol{\varrho}_g(\boldsymbol{y}), \boldsymbol{\psi}_g(\boldsymbol{u})) &= \boldsymbol{R}_{\mathrm{IB}} \boldsymbol{R}_g^{\mathsf{T}} \boldsymbol{S}(\boldsymbol{R}_g \boldsymbol{\omega}) \\ &= \boldsymbol{R}_{\mathrm{IB}} \boldsymbol{R}_g^{\mathsf{T}} \boldsymbol{R}_g \boldsymbol{S}(\boldsymbol{\omega}) \boldsymbol{R}_g^{\mathsf{T}} \\ &= \boldsymbol{f}_{R_{\mathrm{IB}}}(\boldsymbol{x}, \boldsymbol{y}, \boldsymbol{u}) \boldsymbol{R}_g^{\mathsf{T}} \end{aligned} \tag{48.B}$$

In the second line of Eq. (48.B), we have used the property that $\boldsymbol{S}(\boldsymbol{R}\boldsymbol{\omega}) = \boldsymbol{R}\boldsymbol{S}(\boldsymbol{\omega})\boldsymbol{R}^{\mathsf{T}}$ for any $\boldsymbol{R} \in \mathsf{SO}(3)$ and $\boldsymbol{\omega} \in \mathbb{R}^3$. Finally, the angular velocity dynamics are invariant since

$$\boldsymbol{f}_{\omega}(\boldsymbol{\varphi}_g(\boldsymbol{x}), \boldsymbol{\varrho}_g(\boldsymbol{y}), \boldsymbol{\psi}_g(\boldsymbol{u})) = \boldsymbol{I}^{-1} \left(\boldsymbol{I}\boldsymbol{\omega} \times \boldsymbol{\omega} + \boldsymbol{M}_0 + \boldsymbol{M}_v \boldsymbol{v}_{\mathrm{r}} + \boldsymbol{M}_{\omega} \boldsymbol{\omega} \right) = \boldsymbol{f}_{\omega}(\boldsymbol{x}, \boldsymbol{y}, \boldsymbol{u}) \tag{49.I}$$

$$\begin{aligned} \boldsymbol{f}_{\omega}(\boldsymbol{\varphi}_g(\boldsymbol{x}), \boldsymbol{\varrho}_g(\boldsymbol{y}), \boldsymbol{\psi}_g(\boldsymbol{u})) &= (\boldsymbol{R}_g \boldsymbol{I} \boldsymbol{R}_g^{\mathsf{T}})^{-1} \left(\boldsymbol{R}_g \boldsymbol{I} \boldsymbol{R}_g^{\mathsf{T}} \boldsymbol{R}_g \boldsymbol{\omega} \times \boldsymbol{R}_g \boldsymbol{\omega} + \boldsymbol{R}_g \boldsymbol{M}_0 + \boldsymbol{R}_g \boldsymbol{M}_v \boldsymbol{R}_g^{\mathsf{T}} \boldsymbol{R}_g \boldsymbol{v}_{\mathrm{r}} + \boldsymbol{R}_g \boldsymbol{M}_{\omega} \boldsymbol{R}_g^{\mathsf{T}} \boldsymbol{R}_g \boldsymbol{\omega} \right) \\ &= \boldsymbol{R}_g \boldsymbol{I}^{-1} \left(-\boldsymbol{S}(\boldsymbol{\omega}) \boldsymbol{I} \boldsymbol{\omega} + \boldsymbol{M}_0 + \boldsymbol{M}_v \boldsymbol{v}_{\mathrm{r}} + \boldsymbol{M}_{\omega} \boldsymbol{\omega} \right) \\ &= \boldsymbol{R}_g \boldsymbol{f}_{\omega}(\boldsymbol{x}, \boldsymbol{y}, \boldsymbol{u}) \end{aligned} \tag{49.B}$$

□

Acknowledgments

The authors gratefully acknowledge NASA under Grant No. 80NSSC20M0162. The first author thanks Dr. Zakia Ahmed of the Virginia Tech Nonlinear Systems Laboratory for the fruitful discussions on symmetry-preserving observers for wind estimation.

References

[1] Lie, F. A. P., and Gebre-Egziabher, D., "Synthetic Air Data System," *Journal of Aircraft*, Vol. 50, No. 4, 2013, pp. 1234–1249. https://doi.org/10.2514/1.C032177.

[2] Sun, K., Regan, C. D., and Gebre-Egziabher, D., "Observability and Performance Analysis of a Model-Free Synthetic Air Data Estimator," *Journal of Aircraft*, Vol. 56, No. 4, 2019, pp. 1471–1486. https://doi.org/10.2514/1.C035290.

[3] Lawrance, N. R., and Sukkarieh, S., "Path Planning for Autonomous Soaring Flight in Dynamic Wind Fields," *2011 IEEE International Conference on Robotics and Automation*, IEEE, Shanghai, China, 2011, pp. 2499–2505. https://doi.org/10.1109/ICRA.2011.5979966.

[4] Yang, S., and Jeon, S., "Recursive Path Planning and Wind Field Estimation for Precision Airdrop," *Journal of Guidance, Control, and Dynamics*, Vol. 42, No. 6, 2019, pp. 1429–1437. https://doi.org/10.2514/1.G003944.

[5] Gahan, K. C., Hopwood, J. W., and Woolsey, C. A., "Uncertainty in Wind Estimates, Part 1: Analysis Using Generalized Polynomial Chaos," *AIAA SCITECH 2024 Forum*, American Institute of Aeronautics and Astronautics, Orlando, FL, 2024. https://doi.org/10.2514/6.2024-2824.

[6] Hopwood, J. W., and Woolsey, C. A., "Passivity-Based Wind Estimation for Aircraft Maneuvering in Steady and Uniform Wind Fields," *AIAA SCITECH 2024 Forum*, American Institute of Aeronautics and Astronautics, Orlando, FL, 2024. https://doi.org/10.2514/6.2024-2654.

[7] Mahapatra, P., and Zrnic, D., "Sensors and Systems to Enhance Aviation Safety against Weather Hazards," *Proceedings of the IEEE*, Vol. 79, No. 9, 1991, pp. 1234–1267. https://doi.org/10.1109/5.97295.

[8] Stratton, D., and Stengel, R., "Real-Time Decision Aiding: Aircraft Guidance for Wind Shear Avoidance," *IEEE Transactions on Aerospace and Electronic Systems*, Vol. 31, No. 1, 1995, pp. 117–124. https://doi.org/10.1109/7.366298.

[9] Palomaki, R. T., Rose, N. T., van den Bossche, M., Sherman, T. J., and De Wekker, S. F. J., "Wind Estimation in the Lower Atmosphere Using Multirotor Aircraft," *Journal of Atmospheric and Oceanic Technology*, Vol. 34, No. 5, 2017, pp. 1183–1191. https://doi.org/10.1175/JTECH-D-16-0177.1.

[10] Trub, R., Moser, D., Schafer, M., Pinheiro, R., and Lenders, V., "Monitoring Meteorological Parameters with Crowdsourced Air Traffic Control Data," *2018 17th ACM/IEEE International Conference on Information Processing in Sensor Networks (IPSN)*, IEEE, Porto, 2018, pp. 25–36. https://doi.org/10.1109/IPSN.2018.00010.

[11] Jacob, J., Chilson, P., Houston, A., and Smith, S., "Considerations for Atmospheric Measurements with Small Unmanned Aircraft Systems," *Atmosphere*, Vol. 9, No. 7, 2018, p. 252. https://doi.org/10.3390/atmos9070252.

[12] Barbieri, L., Kral, S., Bailey, S., Frazier, A., Jacob, J., Reuder, J., Brus, D., Chilson, P., Crick, C., Detweiler, C., Doddi, A., Elston, J., Foroutan, H., González-Rocha, J., Greene, B., Guzman, M., Houston, A., Islam, A., Kemppinen, O., Lawrence, D., Pillar-Little, E., Ross, S., Sama, M., Schmale, D., Schuyler, T., Shankar, A., Smith, S., Waugh, S., Dixon, C., Borenstein, S., and de Boer, G., "Intercomparison of Small Unmanned Aircraft System (sUAS) Measurements for Atmospheric Science during the LAPSE-RATE Campaign," *Sensors*, Vol. 19, No. 9, 2019, p. 2179. https://doi.org/10.3390/s19092179.

[13] Adkins, K. A., Akbas, M., and Compere, M., "Real-Time Urban Weather Observations for Urban Air Mobility," *International Journal of Aviation, Aeronautics, and Aerospace*, Vol. 7, No. 4, 2020. https://doi.org/10.15394/ijaaa.2020.1540.

[14] Reiche, C., Cohen, A. P., and Fernando, C., "An Initial Assessment of the Potential Weather Barriers of Urban Air Mobility," *IEEE Transactions on Intelligent Transportation Systems*, Vol. 22, No. 9, 2021, pp. 6018–6027. https://doi.org/10.1109/TITS.2020.3048364.

[15] Thipphavong, D. P., Apaza, R., Barmore, B., Battiste, V., Burian, B., Dao, Q., Feary, M., Go, S., Goodrich, K. H., Homola, J., Idris, H. R., Kopardekar, P. H., Lachter, J. B., Neogi, N. A., Ng, H. K., Oseguera-Lohr, R. M., Patterson, M. D., and Verma, S. A., "Urban Air Mobility Airspace Integration Concepts and Considerations," *2018 Aviation Technology, Integration, and Operations Conference*, American Institute of Aeronautics and Astronautics, Atlanta, Georgia, 2018. https://doi.org/10.2514/6.2018-3676.

[16] Karr, D. A., Wing, D. J., Barney, T. L., Sharma, V., Etherington, T. J., and Sturdy, J. L., "Initial Design Guidelines for Onboard Automation of Flight Path Management," *AIAA AVIATION Forum*, VIRTUAL EVENT, 2021. https://doi.org/10.2514/6.2021-2326.

[17] González-Rocha, J., Woolsey, C. A., Sultan, C., and De Wekker, S. F. J., "Sensing Wind from Quadrotor Motion," *Journal of Guidance, Control, and Dynamics*, Vol. 42, No. 4, 2019, pp. 836–852. https://doi.org/10.2514/1.G003542.

[18] Gahan, K., Hopwood, J. W., and Woolsey, C. A., "Wind Estimation Using an H∞ Filter with Fixed-Wing Aircraft Flight Test Results," *AIAA SCITECH 2023 Forum*, American Institute of Aeronautics and Astronautics, National Harbor, MD & Online, 2023. https://doi.org/10.2514/6.2023-2252.

[19] Halefom, M. H., Hopwood, J. W., and Woolsey, C. A., "Unsteady Aerodynamics in Model-Based Wind Estimation from Fixed-Wing Aircraft Motion," *Journal of Guidance, Control, and Dynamics*, Vol. 47, No. 8, 2024, pp. 1556–1568. https://doi.org/10.2514/1.G007836.

[20] Krener, A. J., "The Convergence of the Extended Kalman Filter," *Directions in Mathematical Systems Theory and Optimization*, Vol. 286, edited by A. Rantzer and C. I. Byrnes, Springer Berlin Heidelberg, Berlin, Heidelberg, 2003, pp. 173–182.

[21] Shim, H., Seo, J. H., and Teel, A. R., "Nonlinear Observer Design via Passivation of Error Dynamics," *Automatica*, Vol. 39, No. 5, 2003, pp. 885–892. https://doi.org/10.1016/S0005-1098(03)00023-2.

[22] Chen, H., Bai, H., and Taylor, C. N., "Invariant-EKF Design for Quadcopter Wind Estimation," *2022 American Control Conference (ACC)*, IEEE, Atlanta, GA, USA, 2022, pp. 1236–1241. https://doi.org/10.23919/ACC53348.2022.9867417.

[23] Ahmed, Z., and Woolsey, C. A., "The Invariant Extended Kalman Filter for Wind Estimation Using a Small Fixed-Wing UAV in Horizontal-Plane Flight," *AIAA SCITECH 2024 Forum*, American Institute of Aeronautics and Astronautics, Orlando, FL, 2024. https://doi.org/10.2514/6.2024-2656.

[24] Bonnabel, S., Martin, P., and Rouchon, P., "Symmetry-Preserving Observers," *IEEE Transactions on Automatic Control*, Vol. 53, No. 11, 2008, pp. 2514–2526. https://doi.org/10.1109/TAC.2008.2006929.

[25] Ahmed, Z., Halefom, M. H., and Woolsey, C., "Tutorial Review of Indirect Wind Estimation Methods Using Small Uncrewed Air Vehicles," *Journal of Aerospace Information Systems*, Vol. 21, No. 8, 2024, pp. 667–683. https://doi.org/10.2514/1.I011345.

[26] Hopwood, J., and Woolsey, C., "A Symmetry-Preserving Reduced-Order Observer," *2025 American Control Conference*, Denver, Colorado, 2025. https://doi.org/10.48550/arXiv.2411.07998.

[27] Holm, D. D., Schmah, T., and Stoica, C., *Geometric Mechanics and Symmetry: From Finite to Infinite Dimensions*, Oxford Texts in Applied and Engineering Mathematics, Oxford University Press, New York, 2009.

[28] Boothby, W. M., *An Introduction to Differentiable Manifolds and Riemannian Geometry*, revised second edition ed., Academic Press, San Diego, 2003.

[29] Olver, P. J., *Classical Invariant Theory*, 1st ed., Cambridge University Press, 1999. https://doi.org/10.1017/CBO9780511623660.

[30] Grauer, J. A., and Morelli, E. A., "Generic Global Aerodynamic Model for Aircraft," *Journal of Aircraft*, Vol. 52, No. 1, 2015, pp. 13–20. https://doi.org/10.2514/1.C032888.

[31] Hopwood, J. W., Simmons, B. M., Woolsey, C. A., and Cooper, J. K., "Development and Evaluation of Multirotor Flight Dynamic Models for Estimation and Control," *AIAA SCITECH 2024 Forum*, American Institute of Aeronautics and Astronautics, Orlando, FL, 2024. https://doi.org/10.2514/6.2024-1307.

[32] Rugh, W. J., *Linear System Theory*, 2nd ed., Prentice Hall Information and System Sciences Series, Prentice Hall, Upper Saddle River, N.J, 1996.

[33] Khalil, H. K., *Nonlinear Systems*, 2nd ed., Prentice Hall, Upper Saddle Ridge, New Jersey, 1996.

[34] Hopwood, J. W., and Woolsey, C. A., "A Noise-to-State Stable Reduced-Order Symmetry-Preserving Observer for Wind Estimation," *AIAA SCITECH 2025 Forum*, American Institute of Aeronautics and Astronautics, Orlando, FL, 2025.